Acp-2014-923-revision

Comments, Responses and List of changes in revised manuscript

General Comments from Anonymous referee # 1

This work reports a systematic and rigorous experimental study about hygroscopic behavior of individual particles with sizes < 10µm of a common but important atmospheric system i.e NaCl/NaNO3. Optical microscopy was used to investigate deliquescent and efflorescence of individual particles impacted on hydrophobic substrate for various mixing ratio of NaCl and NaNO3. The change in particle size with the variation of humidity is monitored by measuring the particle areas in the optical images, complementary SEM/EDX measurements were carried out on dried particles to assess the mixing state of individual particles. The experimental results presented by Authors are supported by a well-used thermodynamic model (i.e. AIOMFAC). The introduction is well documented and clearly points out the main difficulties for studying hygroscopicity properties of individual particles. The methodology used here was previously published by Authors (Ahn et al., 2010 and Eom et al., 2014) and has demonstrated its feasibility for investigating hygroscopic behavior of individual particles. <mark>Thus, citation of these articles in the experimental section is lacking</mark>. The results provided by Authors allow building complete DRH and ERH phase diagrams for individual particles with micrometer sizes with mole fraction of NaCl varying from 0.1 to 0.9. Authors clearly demonstrated the hygroscopic behavior as function of the particle composition (i.e. XNaCl = 0.38 (eutonic composition), XNaCl > 0.38 and XNaCl < 0.38) and explain in a very didactic manner the efflorescence and deliquescent behavior of particles step by step during the humidification and dehydration process. Authors evidenced two-stage phase transitions during humidifying process except for the eutonic composition. This is in good agreement with the thermodynamic modeling. The dehydration behavior of particles was also explained by the mixing ratios of the two salts. Interestingly, eutonic composed particles and particles with XNaCl > 0.38 showed two-stage efflorescence transitions while NaNO3 -rich particles showed only a single transition. The microstructure of the dried particles was investigated. SEM/EDX evidenced the core-shell structure of the dried particles which is composed of NaCl in the center and eutonic composed solid shell whatever the initial composition of the particle. Finally, the results are discussed in regards to the atmospheric implication. To our knowledge this is a huge insight in the comprehension of the hygroscopic behavior of individual particles. Actually, this work provides a complete description of the behavior of the particles including particle microstructure during humidifying and dehydration processes. I strongly recommend the publication of the work as is in ACP.

* Response to the general comments by Anonymous Referee #1:
We thank the reviewer very much for the positive evaluation of our work and very insightful comments. We incorporated the references of our previous works in the experimental section as pointed out by the reviewer:
Line # 200-201: (Ahn et al., 2010; Eom et al., 2014);
Line # 206: (Ahn et al., 2010, Li et al., 2014).

Anonymous Referee # 1
However, I have two minor questions: 1- The change in particle size with the variation of RH is

based on optical image analyses meaning that 2D projected areas are taken into account. Since some of particles are not perfectly rounds after crystallization (as seen on SEIs images figure 5), what is the diameter taken into account? feret's diameter?

* Response:
1: The change of particle size (area ratio = A/A0) in the hygroscopic curves plotted both for the humidifying and dehydration processes are with respect to the initial particle area (A0) at the start of the humidifying cycle. These measurements were based on the optical image processing (Matrox, Inspector v9.0) and the final effloresced particle sizes were not integrated with Feret's diameter from SEI-images to keep the consistency of the plot data. This was discussed in detail in our previous publication (Ahn et al., 2010).

Anonymous Referee # 1
2- On figure 2.a we can see that A/A0 of NaNO3-rich particles after efflorescence is larger than 1. This means that the particle size is larger than the initial one at the final step of the process. We cannot observe this behavior for the other mole fractions. Moreover the microstructure of individual particles showed on the figure 5 does not seem to exhibit some differences with NaCl-rich particles. Do the authors have any explanation for this size variation?

* Response:
2: The particle area ratios plotted in Figure 2(a) is with respect to the initial particle area (A0) at the start of the humidifying cycle as pointed out above. As the 2-D projected area ratio was obtained, the different A/A0 values obtained at the start of the humidifying process and at the end of the dehydration process (which would happen due to the deliquescence and efflorescence events) does not necessarily mean that the actual volume (or mass) of the particle (which should be the same) was changed on re-crystallization/solidification (Ahn et al. 2010). The microstructures in SEI images and elemental X-ray maps (Figure 5) clearly complement the efflorescence mechanism of the NaCl-rich and NaNO3-rich and eutonic composed particles (Figure 4). NaCl homogeneously nucleates to crystallize first for all mole fractions and hence forms the core. For NaCl-rich and eutonic composed particles, during the dehydration process the NaCl from the metastable aqueous eutonic part crystallizes at the second ERH (apparently the MERH) on the already crystallized NaCl part (from first ERH). For NaNO3-rich particles, the microstructure is similar because NaCl is homogeneously crystallized in the core and NaNO3 solidifies heterogeneously around the core. We would like to point out that from SEM-EDX mapping (Figure 5) the final microstructure of effloresced NaCl-NaNO3 mixture particles of all mixing ratios show a NaCl core (through homogeneous nucleation) and NaNO3 solidified around that core. This observation is discussed in detail in section 3.5 entitled as: Spatial distribution of effloresced NaCl-NaNO3 solid particles.
Ref: Ahn et al. (2010). "Combined Use of Optical and Electron Microscopic Techniques for the Measurement of Hygroscopic Property, Chemical Composition, and Morphology of Individual Aerosol Particles." Analytical Chemistry 82(19): 7999-8009.

General Comments from Anonymous referee # 2
This paper presents results of very thorough investigation of hygroscopic properties of mixed NaCl/NaNO3 particles. Particles with the broad range of the mixing ratios are systematically

studied experimentally and the results are complemented with thermodynamic modeling. The paper is very well organized, carefully written and previous literature relevant to this study is adequately discussed and meticulously referenced. I recommend publication nearly 'as is', with only minor/editorial suggestions and comments listed below.

* Response to the general comments by Anonymous Referee #2:
We thank the reviewer very much for his/her positive evaluation of our work and helpful suggestions.

Anonymous Referee # 2:
Because accuracy of the RH measurement is +/-0.5%, it does not make sense to report RH values with an accuracy of a tenth percent. I suggest to round up all the reported values to the nearest percent value.

* Response:
The accuracy of the RH measurements in the experimental set-up, i.e. +/-0.5%, was determined by repeated measurements of the DRH of pure NaCl particles. We use the average/mean and standard deviation for the DRH values and error values/bars from repeated humidifying cycles in text and for the deliquescence phase diagram in Figure 3, respectively. For the dehydration process we use the number average and range of ERH values in text and for the efflorescence phase diagram in Figure 4. Hence, we think that the decimal digit in RH representation is not meaningless: for example, we believe that two experimental values such as 76.4(+/-0.5)% and 75.5(+/-0.5)% are different in our experiments, which will be the same as 76(+/-0.5)% if they are rounded as suggested by the reviewer.

Anonymous Referee # 2:
Section 3.2. I think that presenting the eutonic case first (3.2.2) followed by NaCl-rich and NaNO3-rich cases might have some advantage for the text flow and presentation logic.

* Response:
We thank the reviewer for his helpful suggestion in enriching the manuscript flow. Accordingly the section was corrected and rearranged in Line # 265-335 as shown in the marked-up section of the revised manuscript.

Anonymous Referee # 2:
P33145, line 1 and other similar places: use of 'remnant' is somewhat incorrect here. I would avoid using this word.

* Response:
The word "remnant" was "removed" or "replaced" as marked up in the revised manuscript:
Line # 35, 104, 572, and 716 and Figure 6 caption (2 times).

Anonymous Referee # 2:
P33145, line 6: remove 'genuine'

* Response:

In the revised manuscript, line# 40 was modified and "genuine" was removed.

Anonymous Referee # 2:
P33146, line 13 and other similar places: use of word 'full' is unnecessary

* Response:
The word "full" at Line # 72 and 156 was removed in revised manuscript.

Anonymous Referee # 2:
P33152, line 10: replace 'on the other hand' by 'however'

* Response:
Replaced at line # 228 of the revised manuscript.

Anonymous Referee # 2:
P33152, line 20: replace 'exemplar' by 'representative'

* Response:
Replaced at line # 238 of the revised manuscript.

Anonymous Referee # 2:
P33153, line 11: replace 'particular' by 'specific'

* Response:
Replaced at line # 259 of the revised manuscript.

1   **Hygroscopic properties of NaCl and NaNO$_3$ mixture particles as reacted inorganic sea-salt**

2   **aerosol surrogates**

3

4   Dhrubajyoti Gupta, HyeKyeong Kim, Geonhee Park, Xue Li, Hyo-Jin Eom, and Chul-Un Ro[*]

5

6   Department of Chemistry, Inha University, Incheon, 402-751, Korea

7

8

9   **ABSTRACT**

10   NaCl in fresh sea-salt aerosol (SSA) particles can partially or fully react with

11   atmospheric NO$_x$/HNO$_3$, so internally mixed NaCl and NaNO$_3$ aerosol particles can co-exist

12   over a wide range of mixing ratios. Laboratory-generated, micrometer-sized NaCl and NaNO$_3$

13   mixture particles at ten mixing ratios (mole fractions of NaCl (X_{NaCl}) = 0.1 to 0.9) were examined

14   systematically to observe their hygroscopic behavior, derive experimental phase diagrams for

15   deliquescence and efflorescence, and understand the efflorescence mechanism. During the

16   humidifying process, aerosol particles with the eutonic composition (X_{NaCl} = 0.38) showed only

17   one phase transition at their mutual deliquescence relative humidity (MDRH) of 67.9($\pm$0.5)%.

18   On the other hand, particles with other mixing ratios showed two distinct deliquescence

19   transitions, i.e., the eutonic component dissolved at MDRH and the remainder in the solid phase

20   dissolved completely at their DRHs depending on the mixing ratios, resulting in a phase diagram

21   composed of four different phases, as predicted thermodynamically. During the dehydration

22   process, NaCl-rich particles (X_{NaCl} > 0.38) showed two-stage efflorescence transitions: the first

23   stage was purely driven by the homogeneous nucleation of NaCl and the second stage at the

24   mutual efflorescence RH (MERH) of the eutonic components, with values in the range of

25   30.0−35.5%. Interestingly, aerosol particles with the eutonic composition (X_{NaCl} = 0.38) also

26   showed two-stage efflorescence with NaCl crystallizing first followed by heterogeneous

27   nucleation of the remaining NaNO$_3$ on the NaCl seeds. NaNO$_3$-rich particles (X_{NaCl} ≤ 0.3)

28   underwent single-stage efflorescence transitions at ERHs progressively lower than the MERH,

29   because of the homogeneous nucleation of NaCl and the almost simultaneous heterogeneous

[*] Corresponding author. Tel.: +82 32 860 7676; Fax.: +82 32 867 5604; E-mail: curo@inha.ac.kr

nucleation of NaNO$_3$ on the NaCl seeds. SEM/EDX elemental mapping indicated that the effloresced NaCl-NaNO$_3$ particles at all mixing ratios were composed of a homogeneously crystallized NaCl moiety in the center, surrounded either by the eutonic component (for $X_{NaCl} >$ 0.38) or NaNO$_3$ (for $X_{NaCl} \leq 0.38$). During the humidifying or dehydration process, the amount of eutonic composed part drives particle/droplet growth or shrinkage at the MDRH or MERH (second ERH), respectively, and the amount of remnant pure salts (NaCl or NaNO$_3$ in NaCl- or NaNO$_3$-rich particles, respectively) drives the second DRHs or first ERHs, respectively. Therefore, their behavior can be a precursor to the optical properties and direct radiative forcing for these atmospherically relevant mixture particles representing the coarse, reacted inorganic SSAs. In addition, the NaCl-NaNO$_3$ mixture aerosol particles can maintain an aqueous phase over a wider RH range than the genuine pure NaCl particles as SSA surrogate, making their heterogeneous chemistry more probable.

1. Introduction

Atmospheric aerosols play important roles in global climate change, directly by scattering or absorbing incoming solar radiation and indirectly by serving as cloud condensation nuclei (Pandis et al., 1995; Satheesh and Moorthy, 2005). The radiative effects depend on the chemical composition and sizes of the atmospheric aerosol particles. The optical properties and the chemical reactivity of the atmospheric aerosols also depend on their mixing states and different aerosol phases (Martin, 2000). Studies of the hygroscopic properties of inorganic salt particles as aerosol surrogates can provide important insights to several of these important aerosol properties, such as (i) alteration of aerodynamic properties; (ii) cloud-droplet nucleation efficiency; (iii) optical properties; and (iv) physicochemical changes, through complex heterogeneous chemical reactions with atmospheric gas-phase species (Wang and Martin, 2007; Haywood et al., 2000; ten Brink, 1998; Krueger et al., 2003).

Sea-salt or sea-spray aerosols (SSAs) comprise a large proportion of the atmospheric particulate mass (25-50%) (Finlayson-Pitts and Pitts, 2000). Thus far, many studies have examined the hygroscopic behavior of both airborne and laboratory-generated SSAs (Tang et al., 1997; Wise et al., 2007; Wise et al., 2009; Prather et al., 2013), but the hygroscopicity of the SSAs is not completely understood (Meskhidze et al., 2013). NaCl in the nascent SSAs can react

61 quickly (within a few minutes to a hours of residence in air) with the atmospheric NO_x/HNO_3

62 (ten Brink, 1998; Saul et al., 2006; Liu et al., 2007). This can lead to the formation of partially or

63 fully reacted particles containing NaCl and $NaNO_3$ over a range of mixing ratios. Indeed, studies

64 of individual marine aerosols have clearly shown the existence of fully- or partially-reacted SSA

65 particles, and a significant portion of these particles were reported to be mixtures of sodium

66 chloride, nitrate, and/or sulfate (Gard et al., 1998; Ro et al., 2001; Laskin et al., 2003; Ault et al.,

67 2014). Moreover, the further reactive uptake of N_2O_5 was reported to be dependent on the

68 chloride to nitrate ratio of the reacted SSAs and their phases (Ryder et al., 2014). The primary

69 and secondary organics, biogenic particulates, sea-salt sulfates (ss-SO_4^{2-}), non-sea-salt sulfates

70 (nss-SO_4^{2-}), etc., add greater complexity to these SSAs (O'Dowd and de Leeuw, 2007; Keene et

71 al., 2007; Prather et al., 2013; Beardsley et al., 2013; Ault et al., 2013b). A detailed knowledge of

72 the full hygroscopic properties, mixing states, and the spatial distribution of the chemical

73 components in NaCl-$NaNO_3$ mixture particles, as partially or fully reacted SSA surrogates, can

74 serve as a good preliminary step to a better understanding of the complex chemical/physical

75 mixing states, hygroscopic behavior, and reactivity of ambient SSAs.

76 Many studies have examined the hygroscopic properties of two-component inorganic

77 salt particles as inorganic aerosol surrogates (Cohen et al., 1987a; Tang and Munkelwitz, 1993,

78 1994a, 1994b; Tang et al., 1978; Ge et al., 1996; Ge et al., 1998; Chang and Lee, 2002). Stepwise

79 phase transitions generally occur for particles composed of two inorganic salts during the

80 humidifying process (Wexler and Seinfeld, 1991). On the other hand, particles with the eutonic

81 composition deliquesce completely at the mutual deliquescence relative humidity (MDRH),

82 resulting in a single phase transition. For two-component inorganic hygroscopic salt particles, the

83 first transition generally occurs at their MDRH, and the aqueous phase resulting from the partial

84 deliquescence has the eutonic composition. The residual solid component keeps absorbing water

85 with further increases in the RH and completely dissolves when the RH reaches their DRH,

86 which depends on the composition of the particle. As the humidifying processes of inorganic

87 salts are governed by thermodynamics, a range of thermodynamic models have been developed

88 to predict the deliquescence behavior or the ionic activity coefficients of two-component aerosol

89 particles (Tang, 1976; Ansari and Pandis, 1999; Clegg et al., 1998; Wexler and Clegg, 2002;

90 Zuend et al., 2008, 2011). The Extended Atmospheric Inorganic Model (E-AIM) predicts the

91 physical state and chemical compositions of aerosols containing several atmospherically relevant

서식 있음: 취소선

inorganic ionic species and/or organic species (http://www.aim.env.uea.ac.uk/aim/aim.php). The Aerosol Inorganic-Organic Mixtures Functional group Activity Co-efficient (AIOMFAC) model allows calculations of the activity coefficients in organic and/or inorganic mixtures from simple binary solutions to complex multicomponent systems (http://www.aiomfac.caltech.edu). On the other hand, there have been few systematic, experimental hygroscopic studies to support the theoretical models for mixed salt particles.

During the dehydration process, where the RH is decreased from high to low, the concentration of single salts in the aqueous droplets becomes dense and the inorganic single salts can be finally crystallized at their efflorescence RH (ERH). The ERH is sometimes significantly lower than the DRH. For example, pure NaCl particles have a DRH of ~75% and ERH of ~45-47% (Martin, 2000). From a thermodynamic point of view, or as observed in bulk ternary systems, aqueous droplets with double salts should show step-wise efflorescence transitions: a component in the aqueous droplets precipitates first at their ERH and then the remnant aqueous phase of the eutonic composition effloresces at their mutual ERH (MERH), which should be lower than either ERHs of the pure salts. Therefore, effloresced mixed particles may form a heterogeneous, core-shell crystal structure owing to the step-wise crystallization process (Ge et al., 1996). On the other hand, aqueous droplets with a eutonic composition are expected to crystallize simultaneously, resulting in a homogeneous crystal structure. Efflorescence, however, is a kinetic or rate-driven process that requires a sufficient activation energy to overcome the kinetic barrier (Martin, 2000). This kinetic or critical-nucleation barrier in turn depends on a range of factors, such as the mixing states of the chemical components, micro-physical states, supersaturation levels, vapor pressure, interfacial tension, viscosity, inter-ionic forces, and solute-water and solute-solute interactions (Cohen et al., 1987b). Therefore, the ERHs of single or multi-component salts are difficult to predict theoretically (Seinfeld and Pandis, 2006). A theoretical model for the efflorescence behavior of the $NaCl-Na_2SO_4$ mixed system was reported, where the efflorescence was considered to be driven primarily by the homogeneous nucleation of the more supersaturated salt, resulting in a sufficiently large seed for the subsequent heterogeneous nucleation of the other salt (Gao et al., 2007). However, there is no general model that covers the efflorescence of multi-component particles because it depends on many complicated parameters and varies with the salt characteristics. Therefore, the best way to understand the efflorescence behavior of aerosols is through experimental measurements

8

123   (Seinfeld and Pandis, 2006). For example, a recent experimental study of the two component
124   NaCl-KCl mixture particles showed that during the dehydration process, the aqueous droplets of
125   various mixing ratios underwent single step efflorescence (Li et al., 2014). Based on the
126   experimentally-obtained efflorescence phase diagram and X-ray elemental maps of the
127   effloresced NaCl-KCl mixture particles at various mixing ratios, it was suggested that the more
128   supersaturated salt nucleated homogeneously to crystallize in the center and the other salt
129   underwent heterogeneous crystallization on the former almost simultaneously in the time-scale
130   of the measurements. Full phase diagrams, covering the entire range of mixing ratios, are needed
131   to fully understand the hygroscopic behavior of multi-component aerosol particles (Martin,
132   2000).

133   Up until now, there have been only a few studies on the hygroscopic properties of mixed
134   NaCl-NaNO$_3$ aerosol system. Tang and Munkelwitz (1994a) examined the temperature
135   dependent deliquescence behavior of equi-molar mixed NaCl-NaNO$_3$ particles using a single-
136   particle levitation technique. Ge et al. (1998) also studied the deliquescence behavior of mixed
137   NaCl-NaNO$_3$ particles with a NaCl mole fraction of 0.2, 0.378 (eutonic), and 0.8 using rapid
138   single-particle mass spectrometry (RSMS), where only MDRH was measured experimentally
139   and it was claimed that the second-stage DRHs agreed with the thermodynamic predictions of
140   AIM. Although the crystallization process was not studied experimentally, a core-shell type of
141   heterogeneous morphology in the NaCl-NaNO$_3$ particles was proposed based on the two-step
142   deliquescence phase transitions observed during the humidifying process (Ge at al., 1998;
143   Hoffmann et al, 2004) and by measuring the secondary electron yields from the nebulized
144   mixture particles (Ziemann and McMurry, 1997). On the other hand, as observed for the NaCl-
145   KCl mixture particles, particles that exhibit two-step deliquescence phase transitions do not
146   always have a core-shell type (Li et al., 2014). Moreover, it was reported that pure NaNO$_3$
147   droplets do not crystallize easily during the dehydration process, and at very low RHs they
148   appear to exist in an amorphous form (Hoffmann et al, 2004; Gibson et al., 2006; Kim et al.,
149   2012). Therefore, the mixing states in NaCl-NaNO$_3$ particles can be understood only when the
150   efflorescence phenomena for these mixture particles are elucidated. In this study, the hygroscopic
151   properties and microstructure of mixed NaCl-NaNO$_3$ particles at various mixing ratios were
152   examined extensively by optical microscopy and scanning electron microscopy/energy dispersive
153   X-ray spectroscopy (SEM/EDX). The phase transitions of the mixed NaCl-NaNO$_3$ aerosol

9

particles were observed by monitoring the size changes of the particles on the optical images as a function of the RH. SEM/EDX mapping was used to investigate the compositional distribution in the effloresced particles. This paper describes the ~~full~~ hygroscopic behavior of the NaCl-NaNO$_3$ binary aerosol particles as reacted SSA surrogates at ten different mixing ratios for the first time.

2. Experimental Section

2.1. Preparation of mixed NaCl-NaNO$_3$ particles

Mixed NaCl-NaNO$_3$ particles were generated by the nebulization of mixed aqueous solutions. Pure solutions (1.0 M) of NaCl and NaNO$_3$ (NaCl, >99.9% purity, Aldrich; NaNO$_3$, 99.9% purity, Aldrich) were prepared and the desired solution was made by mixing the two solutions volumetrically. A single jet atomizer (HCT4810) was used to generate aerosol particles to be deposited on TEM grids (200 mesh Cu coated with Formvar stabilized with carbon, Ted Pella, Inc.), which behave as hydrophobic substrates (Eom et al., 2014). The aqueous aerosol particles were dried by passing through a silica packed diffusion dryer (HCT4920) with a residence time of ~2 s. The size of the dry particles ranged from 1 to 10 μm.

In this study, NaCl-NaNO$_3$ particles with 10 different mixing ratios were investigated; i.e., 9 compositions with NaCl mole fractions of 0.1−0.9 (X_{NaCl} = 0.1, 0.2, 0.3, 0.4, 0.5, 0.6, 0.7, 0.8, and 0.9, where X_{NaCl} represents the mole fraction of NaCl.) and a eutonic composition (X_{NaCl} = 0.378 ≈ 0.38, which was calculated from the ionic activity products predicted by the AIOMFAC model). Based on the mixing ratio of two salts, the mixed NaCl-NaNO$_3$ particles were divided into three categories: (1) eutonic particles (X_{NaCl} = 0.38), (2) NaCl-rich particles containing larger NaCl fraction than the eutonic composition (X_{NaCl} > 0.38), and (3) NaNO$_3$-rich particles containing larger NaNO$_3$ fraction than the eutonic composition (X_{NaCl} < 0.38).

2.2. Hygroscopic Property Measurement

The hygroscopic properties of the particles were investigated using a "see-through" inertia impactor apparatus equipped with an optical microscope. The experimental set-up is described in detail elsewhere (Ahn et al., 2010). Briefly, the apparatus is composed of three parts: (A) see-through impactor, (B) optical microscope and (C) humidity controlling system. A TEM grid on

184 which aerosol particles were deposited was mounted on the impaction plate in the see-through

185 impactor. The RH inside the impactor was controlled by mixing dry and wet (saturated with

186 water vapor) N_2 gases. The wet N_2 gas was obtained by bubbling through deionized water

187 reservoirs. The flow rates of the dry and wet N_2 gases were controlled by mass flow controllers

188 to obtain the desired RH in the range of ~ 3 − 93%, which was monitored using a digital

189 hygrometer (Testo 645). The digital hygrometer was calibrated using a dew-point hygrometer

190 (M2 Plus-RH, GE), providing RH readings with ±0.5% reproducibility. To achieve a steady state

191 for condensing or evaporating water, each humidity condition was sustained for at least two

192 minutes. The particles on the impaction plate were observed through a nozzle throat using an

193 optical microscope (Olympus, BX51M). Images of the particles were recorded continuously

194 using a digital camera (Canon EOS 5D, full frame, Canon EF f/3.5 L macro USM lens) during

195 the humidifying (by increasing RH from ~3 to ~93%) and dehydration (by decreasing RH from

196 ~93 to ~3%) experiments. The image size was 4368 × 2912 pixels and the image recording

197 condition was set to ISO200. The exposure time was 0.4 s, and the DOF was F/3.5. All

198 hygroscopic experiments were conducted at room temperature (T=22±1 ^{o}C).

199   The change in particle size with the variation of RH was monitored by measuring the

200 particle areas in the optical images. The particle images were processed using image analysis

201 software (Matrox, Inspector v9.0). The size of the imaging pixel was calibrated using 10 μm

202 Olympus scale bars. Particles with $D_p > 0.5$ μm could be analyzed using the present system (Ahn

203 et al., 2010; Eom et al., 2014).

204

205 **2.3. SEM/EDX Measurement**

206   After the hygroscopicity measurements of the individual particles, SEM/EDX was

207 performed for the effloresced particles to determine the morphology and spatial distribution of

208 the chemical elements (Ahn et al., 2010; Li et al., 2014). The measurements were carried out

209 using a Jeol JSM-6390 SEM equipped with an Oxford Link SATW ultrathin window EDX

210 detector. The resolution of the detector was 133 eV for the Mn Kα X-rays. The X-ray spectra and

211 elemental maps were recorded under the control of Oxford INCA Energy software. A 10 kV

212 accelerating voltage and 0.2 nA beam current was used and the typical measuring times were 10

213 min. for elemental mapping.

214

3. Results and Discussion

215

216

3.1 Hygroscopic behavior of pure NaCl and NaNO$_3$ particles

217

218   Aerosol particles generated from a pure NaCl aqueous solution showed typical

219 hysteresis curves with DRH = 75.5($\pm$0.5)% and ERH = 47.6 − 46.3%, and these values were

220 consistent with the reported values (Wise et al., 2007; Tang et al., 1997). The DRH and ERH of

221 the single-component NaCl aerosol particles are denoted as those of the "pure NaCl limit". The

222 dry-deposited NaNO$_3$ powder particles exhibited typical hygroscopic curves with definite phase

223 transitions at DRH = 74.0($\pm$0.5)%, and ERH = 45.7 − 26.7%, which are similar to the values

224 reported by Tang and Munkelwitz (1994b). Hereafter, the DRH of the "pure NaNO$_3$ limit" is

225 defined as 74.0%. On the other hand, most wet deposited aerosol particles (> 90%) generated by

226 nebulization from a NaNO$_3$ aqueous solution grew continuously and shrank without any phase

227 transition during the humidifying and dehydration processes, which have also been reported

228 (Gysel et al., 2002; McInnes et al., 1996; Lee et al., 2000; Hoffman et al., 2004). However, a few

229 wet deposited particles showed ERH in the range, 25.8 − 18.9%. This discrepancy was attributed

230 to the different nucleation mechanisms, i.e. homogeneous and heterogeneous nucleation, for pure

231 and impure (seed containing) NaNO$_3$ particles, respectively. Detailed discussions can be found

232 elsewhere (Kim et al., 2012). Nebulized NaNO$_3$ particles may exist as amorphous particles with

233 no visible ERHs (Hoffmann et al., 2004; Kim et al., 2012).

234

3.2 Hygroscopic behavior of mixed NaCl-NaNO$_3$ particles

235

236   To describe the measurement procedure for observing the hygroscopic behavior of

237 individual aerosol particles during humidifying and dehydration processes, Fig. 1 presents

238 representative optical images of NaCl-NaNO$_3$ particles with a NaCl-rich composition, i.e., X_{NaCl}

239 = 0.8, taken at various RHs. Images (a−e) and (f−j) were recorded when the RH was first

240 increased ($\uparrow$) from ~ 3% to 90% (humidifying process), and then decreased ($\downarrow$) from ~ 90% to

241 3% (dehydration process), respectively. As the optical images of the particles were recorded

242 using a digital camera, the data for 10 − 15 particles in each image field was obtained. During the

243 humidifying process, the sizes and shapes of the particles did not change until all the particles

삭제됨:

삭제됨: On the other hand

삭제됨: exemplar

12

247 absorbed moisture and showed a first partial deliquescence transition at RH = 67.9(±0.5)%,

248 which is the DRH of the eutonic composed part (i.e., $X_{NaCl} = 0.38$) (see Fig. 2c). Upon further

249 increases in RH, the particles absorbed more moisture and grew in size until a second

250 deliquescence transition occurred at RH = 73.7%, where all the particles were fully converted to

251 homogeneous aqueous droplets. After the second deliquescence transition, liquid droplets

252 underwent hygroscopic growth with increasing RH due to the condensation of water vapor.

253 During the dehydration process, the aqueous droplets decreased gradually in size, until the first

254 efflorescence transitions were observed over the range of RH = 45.2 – 44.7% for different

255 droplets in the image field, where they became partially crystallized. Upon further decreases in

256 RH, they underwent a second and final efflorescence transition over the range of RH = 33.5 –

257 30.0%. All particles in the image field were finally transformed into solids at RH = 30.0%, below

258 which no further decrease in size was observed. All the particles in the image field showed two

259 stage deliquescence transitions at specific RHs because the deliquescence transitions are prompt.

260 On the other hand, the two stage efflorescence transitions occurred over a range of RH because

261 the efflorescence driven by the nucleation kinetics is a stochastic process (Martin, 2000; Krieger

262 et al., 2012). As the projected optical image of a particle placed on the substrate was monitored

263 during the hygroscopic measurements, the shape and size of the effloresced particles did not

264 appear the same as the original dry particle due to the rearrangement of a solid particle when it

265 crystallizes during the dehydration process.

266   Figure 2 presents the humidifying and dehydration curves for mixed NaCl-NaNO$_3$

267 particles at different mixing ratios. The humidifying and dehydration curves are represented as

268 the area ratio (A/A$_o$: left-hand axis), which was obtained by dividing the 2D projected particle

269 area at a given RH (A) by that before starting the humidifying process (A$_o$). The hygroscopic

270 behavior of the mixed NaCl-NaNO$_3$ particles differed according to the categories, i.e. eutonic,

271 NaCl-rich, and NaNO$_3$-rich particles, which are discussed in the next sections.

272

3.2.1 Eutonic particles ($X_{NaCl} = 0.38$)

274   Fig. 2c shows the 2D projected area ratio plot as a function of the RH obtained during

275 humidifying and dehydration processes for a representative eutonic particle. During the

276 humidifying process, a single phase transition from solid particles to liquid droplets was

13

삭제됨: particular

삭제됨: NaCl-rich,

observed at RH = 67.1−67.9%. After deliquescence, the size of the liquid droplet grew gradually and continuously with further increases in RH. As the eutonic particles deliquesced at RH = 67.9(±0.5)%, they approached the MDRH of the mixed NaCl-NaNO$_3$ particles. The measured MDRH is consistent with the value calculated from the ionic activity products predicted by the AIOMFAC model and other experimental values (Tang and Munkelwitz, 1994a). During the dehydration process, however, the eutonic droplets showed two stage efflorescence transitions. The particle (Fig. 2c) decreased gradually in size due to water evaporation and the particle size decreased sharply at the first efflorescence transition at RH = 37.3 − 36.6%.　The particle was then observed to undergo a second efflorescence transition at RH = 35.3 − 34.4%. All eutonic droplets in the optical image field showed first and second ERHs over the range of RH = 37.7 − 35.7% and 35.4 − 33.4%, respectively.

In general, the effloresced particle areas are different from the original ones; i.e., the A/A_0 values deviate from unity (see Fig. 2) due to the rearrangement of the particles during recrystallization. Because only the top-view 2D images are obtained from particles sitting on the substrate, the morphology of the particles may not appear the same after recrystallization unless they are perfectly spherical.

3.2.2 NaCl-rich particles ($X_{NaCl} > 0.38$)

Fig. 2e presents the 2D-area ratio plot as a function of the RH of a NaCl-rich particle ($X_{NaCl} = 0.8$). During the humidifying process, the particle size remained constant until RH = ~ 65.5%, where a slight decrease in size was observed due to water adsorption in the lattice imperfections of the solid salts in the particle and structural rearrangement inside the crystal lattice. A first deliquescence transition was observed from RH = 67.7% to 68.0%, where its size increased sharply. With further increases in RH, it grew gradually until RH = 73.7%, at which point the second transition occurred. Thereafter, with further increases in RH, the particle grew continuously. The first phase transition at RH = 68.0%, i.e., MDRH (RH = 67.9(± 0.5)%) of the NaCl-NaNO$_3$ system, was assigned to the deliquescence of the eutonic component in the particle. At the MDRH, the particle consisted of a mixed phase of liquid droplets (eutonic solution) and NaCl solid inclusion. The solid inclusions in the partially deliquesced mixed inorganic salt particles were also observed by environmental transmission electron microscopy (ETEM)

310 (Freney et al. 2009, 2010). Above the MDRH, with the increase in RH, the condensed water kept
311 dissolving the NaCl solid inclusion, and NaCl solid dissolved thoroughly at RH = 73.7%, which
312 is the second DRH of the particles with $X_{NaCl} = 0.8$.

313   All other NaCl-rich particles with different compositions (e.g., $X_{NaCl} = 0.5$ and 0.9 in Fig.
314 2d and 2f, respectively) also exhibited two-stage phase transitions during the humidifying
315 process: the first transition at MDRH (RH = 67.9(±0.5)%) due to deliquescence of the eutonic
316 component and the second one at their DRHs owing to complete deliquescence of the particles.
317 The MDRH is independent of the particle composition. On the other hand, the DRHs are
318 dependent on the compositions and shift toward the a pure NaCl limit (DRH = 75.5(±0.5)%)
319 with increasing NaCl mole fraction. Fig. 3 plots the measured DRHs for the NaCl-rich particles
320 with various compositions as a function of the NaCl mole fraction, showing that the
321 experimental DRH values are in good agreement with the values calculated from the AIOMFAC
322 model.

323   During the dehydration process (Fig. 2e), a representative NaCl-rich particle with the
324 composition of $X_{NaCl} = 0.8$ shows two-stage phase transition. The liquid droplet gradually
325 decreased in size with decreasing RH and became supersaturated by NaCl below 73.7% RH
326 (DRH for $X_{NaCl} = 0.8$). With the further decreases in RH, the droplet size decreased sharply at
327 RH = 46.6 − 45.1% due to the crystallization of NaCl in the droplet. At RH = 45.1%, the first
328 ERH for $X_{NaCl} = 0.8$, the particle was composed of a mixed phase of eutonic solution and NaCl
329 solid. With further decreases in RH, the eutonic component in the particle precipitated at RH =
330 32.2%, which is the MERH of the aerosol particle, resulting in the formation of a completely
331 effloresced solid particle. The measured first ERH and MERH for the particles with a
332 composition of $X_{NaCl} = 0.8$ varied among the particles and were in the range, RH = 45.2 − 44.7%
333 and RH = 33.5 − 30.0%, respectively. All other NaCl-rich particles with different compositions
334 also exhibited two-stage transitions during the dehydration process: the first transition at their
335 ERH, which is specific to their compositions, owing to the homogeneous nucleation and
336 crystallization of NaCl, and the second transition at the MERH due to precipitation of the eutonic
337 component.

338   As the NaCl-rich particles show two-stage phase transitions during the dehydration
339 process, they may form a core-shell type structure where the crystalline NaCl occupies the center

삭제됨: In general, the effloresced particle areas are different from the original ones; i.e., the A/A₀ values deviate from unity (see Fig. 2) due to the rearrangement of the particles during recrystallization. Because only the top-view 2D images are obtained from particles sitting on the substrate, the morphology of the particles may not appear the same after recrystallization unless they are perfectly spherical. .

352 and the eutonic solid is present at the surface. Detailed microstructures of the effloresced NaCl-

353 rich particles will be discussed later.

354

3.2.3 NaNO$_3$-rich particles (X_{NaCl} < 0.38)

356   All NaNO$_3$-rich particles also showed two-stage transitions during the humidifying

357 process. For example, in Fig. 2b, a NaNO$_3$-rich particle with the composition of X_{NaCl} = 0.2

358 showed the first and second transition at RH = 67.5 − 67.9% (MDRH) and RH = 71.2%,

359 respectively. At the MDRH, the deliquesced component formed a eutonic aqueous solution and

360 the un-deliquesced NaNO$_3$ solid was still included in the eutonic solution. Above MDRH, the

361 aerosol particle absorbed water continuously with a further increase in the RH, and it deliquesced

362 completely at RH = 71.2%, which is the second DRH of the particle of X_{NaCl} = 0.2. Above DRH,

363 the size of the liquid droplet increased with increasing RH due to the condensation of water

364 vapor. Other NaNO$_3$-rich particles (e.g., X_{NaCl} = 0.1 in Fig. 2a) also exhibited two-stage phase

365 transitions during the humidifying process: the first transition at MDRH due to the deliquescence

366 of the eutonic component (independent of chemical composition) and the second one at their

367 DRH due to the complete deliquescence of the particles. In all NaNO$_3$-rich particles, the second

368 DRH was dependent on the mixing ratio of the particles and shifted toward the pure NaNO$_3$ limit

369 (DRH of NaNO$_3$ = 74.0 (±0.5)%) with increasing NaNO$_3$ mole fraction (Fig. 3).

370   The hygroscopic behavior of the NaNO$_3$-rich particles during the dehydration process

371 was different from that of NaCl-rich particles. The NaCl-rich particles showed two-stage

372 transitions, whereas the NaNO$_3$-rich particles showed a single-stage transition. For example, a

373 droplet of X_{NaCl} = 0.2 decreased continuously in size with decreasing RH until it showed an

374 efflorescence transition at RH = 29.4 − 29.2% (Fig. 2b). Similar to the NaCl-rich case, the

375 NaNO$_3$-rich particles would be expected to exhibit two-stage transitions during the dehydration

376 process, i.e., the first transition accompanying the precipitation of solid NaNO$_3$, and the second

377 one due to the efflorescence of the eutonic component. However, all the NaNO$_3$-rich particles

378 with X_{NaCl} = 0.1, 0.2, and 0.3 showed single-stage efflorescence transitions during the

379 dehydration process (Figs. 2a, 2b, and 4), suggesting that all the components in the NaNO$_3$-rich

380 particles crystallized (almost) simultaneously. The supersaturated NaNO$_3$ in the droplets did not

381 appear to crystallize until the NaCl crystallized and acted as heterogeneous nuclei for the almost

16

420   simultaneous solidification of $NaNO_3$. To confirm this assumption, particles with small fractions

421   of NaCl, such as particles with X_{NaCl} = 0.01, 0.03, and 0.05, were investigated. The particles with

422   X_{NaCl} = 0.05 showed two-stage and single-stage transitions during the humidifying and

423   dehydration processes, respectively, which is similar to that observed with the $NaNO_3$-rich

424   particles with a composition of $X_{NaCl} \geq 0.1$. On the other hand, the particles with X_{NaCl} = 0.01 and

425   0.03 underwent continuous hygroscopic growth and shrinkage without phase transitions during

426   the humidifying and dehydration processes, respectively, which is similar to that of aerosol

427   particles generated from an aqueous single-component $NaNO_3$ solution. Pure nebulized $NaNO_3$

428   did not show clear efflorescence transitions apparently because of its amorphous nature

429   (Hoffman et al., 2004; Gibson et al., 2006; Kim et al., 2012). Therefore, a sufficient quantity of

430   heterogeneous nuclei (NaCl in this case) is needed to induce the crystallization of $NaNO_3$. A

431   similar observation was reported for the crystallization of NH_4NO_3 and NH_4HSO_4 aerosol

432   particles (Schlenker and Martin, 2005). Both the pure one-component salts did not effloresce,

433   even at RH = 1% and their crystallization could be promoted with the addition of some fraction

434   of inclusions that could serve as good heterogeneous nuclei.

435

436   **3.3 Deliquescence phase diagram of mixed NaCl-NaNO₃ particles**

437   Fig. 3 presents the measured MDRHs (the first DRHs) and second DRHs of the NaCl-

438    $NaNO_3$ mixture particles with different mole fractions along with the measured DRHs of the

439   pure NaCl and $NaNO_3$ particles. As shown in Fig. 3, a clearly demarked phase diagram depicting

440   their deliquescence behavior was obtained experimentally; i.e.,

441   (i) $NaCl(s)$ + $NaNO_3(s)$ phase in Fig. 3: both NaCl and $NaNO_3$ are mixed as solids below the

442   MDRH at all mole fractions;

443   (ii) $NaCl(s)$ + eutonic(aq) phase: a mixed phase of solid NaCl and aqueous eutonic

444   components between the MDRH and second DRHs for $X_{NaCl} > 0.38$;

445   (iii) $NaNO_3(s)$ + eutonic(aq) phase: a mixed phase of solid $NaNO_3$ and aqueous eutonic

446   components between the MDRH and second DRHs for $X_{NaCl} < 0.38$; and

447   (iv) $NaCl(aq)$ + $NaNO_3(aq)$ phase: both NaCl and $NaNO_3$ are mixed in the aqueous phase

448   above the second DRHs at all mole fractions.

449   This MDRH and second DRHs obtained experimentally agrees well with the values

17

450   calculated from the ionic activity products of constituents predicted by the AIOMFAC model, as

451   shown in Fig. 3 (dotted line for MDRH and dotted curve for the second DRHs). Although many

452   theoretical models have been developed to predict the hygroscopic behavior of a mixed sodium

453   chloride and nitrate system (Tang, 1976; Ansari and Pendis, 1999; Clegg et al., 1998; Wexler and

454   Clegg, 2002), only a few experimental results have been reported. Tang and Munkelwitz (1994a)

455   reported an MDRH = 68.0($\pm$0.4)% at 25 °C. Ge et al. (1998) examined the deliquescence

456   behavior of mixed NaCl-NaNO$_3$ particles with a NaCl mole fraction of 0.2, 0.38(eutonic), and

457   0.8, using RSMS. They claimed that the DRHs were generally consistent with the AIM

458   thermodynamic model predictions. On the other hand, the measured DRH values were not

459   reported except for the MDRH of 67.0%, which was lower than the 67.9% obtained in the

460   present study, because the RSMS appeared to detect only the start of the transition similar to the

461   present system where mutual deliquescence for X_{NaCl} = 0.38 began at 67.1 % (Fig. 2b), whereas

462   the actual MDRH was at the end of the transition at 67.9 % when the eutonic particle dissolved

463   completely.

464   All the mixed NaCl-NaNO$_3$ particles showed the first phase transition at the MDRH

465   regardless of the mixing ratio of the two salts. Thermodynamically, as the phase transition of

466   mixed-salts is governed by the water activity at the eutonic point, the MDRH of the mixed-salt

467   particles is independent of the initial composition of the mixture. Other inorganic mixed particles,

468   such as NaCl-KCl, Na$_2$SO$_4$-NaNO$_3$ and NH$_4$Cl-NaCl particles, also exhibited a mutual

469   deliquescence transition at RHs, which were independent of the initial dry-salt compositions, and

470   the phase diagram followed the typical pattern for these two-component inorganic salt + water

471   ternary systems (Tang and Munkelwitz, 1994a; Li et al., 2014; Kelly et al., 2008). For the NaCl-

472   rich particles of X_{NaCl} > 0.38, which contain more NaCl than the eutonic composition, the second

473   DRH value approached the DRH of the pure NaCl salt as the NaCl concentration was increased.

474   For the NaNO$_3$-rich particles of X_{NaCl} < 0.38, the DRH approached that of pure NaNO$_3$ as the

475   NaNO$_3$ mole fraction was increased (Fig. 3). This suggests that the second-stage deliquescence is

476   purely driven by the solid salt remaining after the first deliquescence of the eutonic composition.

477

478   **3.4 Efflorescence phase diagram of mixed NaCl-NaNO$_3$ particles**

479   Fig. 4 shows the measured ERHs and MERHs for the mixed NaCl-NaNO$_3$ particles with

480   various mixing ratios as a function of the NaCl mole fraction. Unlike the deliquescence phase

481   diagram, which showed four systematic phases, the efflorescence phase diagram is composed of

482   three distinct phases; i.e.,

483   (i) $NaCl(aq) + NaNO_3(aq)$ phase: both NaCl and $NaNO_3$ are mixed in the aqueous phase

484   above the first ERHs at all mixing ratios;

485   (ii) $NaCl(s)$ + eutonic(aq) phase: a mixed phase of solid NaCl and aqueous eutonic

486   components between the first ERH and second ERH (MERH) for $X_{NaCl} \geq 0.38$; and

487   (iii) $NaCl(s) + NaNO_3(s)$ phase: both NaCl and $NaNO_3$ are mixed as solids below the second

488   ERH (MERH) for $X_{NaCl} \geq 0.38$ and below the first ERHs for $X_{NaCl} < 0.38$.

489   This experimental phase diagram for efflorescence is reported for the first time, for which no

490   theoretical predictions or other experimental reports exist to the best of the authors' knowledge.

491   The ERH of NaCl-rich droplets ($X_{NaCl} > 0.38$) shifted toward the pure NaCl limit (RH =

492   47.6 − 46.3%) when the NaCl content was increased (see Fig. 4). The measured MERH was

493   observed at a relatively wide range of RH = 30.0 − 35.5%. The droplets with the eutonic

494   composition ($X_{NaCl} = 0.38$) showed the first and second ERHs (MERH) over a range of 37.7 −

495   35.7% and 35.4 − 33.4%, respectively. The $NaNO_3$-rich droplets ($X_{NaCl} < 0.38$) had only one

496   stage efflorescence transition and the decreasing trend of their ERHs as the NaCl mole fraction

497   was decreased clearly follows that for the NaCl-rich and eutonic droplets (Fig. 4). This suggests

498   that the first efflorescence of the NaCl-$NaNO_3$ mixture droplets at all mixing ratios is driven by

499   the homogeneous nucleation of NaCl. For the NaCl-rich droplets, crystallized NaCl acts as a

500   seed for further precipitation of the remaining metastable eutonic aqueous part. For the eutonic

501   droplets, NaCl is crystallized homogeneously at the first ERH and the remaining $NaNO_3$ solidify

502   heterogeneously on the NaCl seeds at the second ERH. For $NaNO_3$-rich droplets, due to the low

503   NaCl content, the homogeneous nucleation rate of NaCl decreases with decreasing NaCl mole

504   fraction, and the $NaNO_3$ appears to undergo almost simultaneous heterogeneous crystallization

505   (precipitation) on the NaCl seeds under the time scale of measurements (i.e., within 2 minutes of

506   the equilibrating time for recording images during the first observed efflorescence transition).

507

508   **3.5 Spatial distribution of effloresced NaCl-NaNO$_3$ solid particles**

509   To examine the morphology and spatial distribution of the chemical components in

510   NaCl-NaNO$_3$ particles at various mixing ratios, SEM/EDX were performed for the effloresced
511   solid particles formed after the humidifying and dehydration cycles. Fig. 5(a) shows the
512   secondary ion image (SEI) and elemental X-ray mapping images of a NaCl-rich (X_{NaCl} = 0.8)
513   particle. The elemental X-ray maps suggest that Cl (from NaCl) is concentrated in the central
514   part, whereas O (from NaNO$_3$) is more concentrated at the edges. This suggests that NaCl
515   nucleates homogeneously to crystallize in the center at the first ERH, whereas NaCl and NaNO$_3$
516   from the eutonic phase crystallized on these central NaCl seeds and precipitated on the edges at
517   the second ERH (MERH), respectively.

518   For a typical particle with a eutonic composition (X_{NaCl} = 0.38), the elemental map of Cl
519   suggests that NaCl is again more concentrated at the central part like NaCl-rich particles and O
520   from NaNO$_3$ is concentrated around this NaCl core (Fig. 5(b)), suggesting that NaCl is nucleated
521   homogeneously to crystallize in the center at the first ERH, whereas the remaining NaNO$_3$
522   precipitated at the second ERH. The thermodynamically-expected, homogeneously-mixed
523   eutonic particles were not observed, and the spatial distribution was rather ruled by the two stage
524   efflorescence transitions.

525   In the case of NaNO$_3$-rich particles, as shown in Fig. 5(c), the Cl component was
526   localized in the core region, and Na and O are distributed over the entire particle. This suggests
527   that even for NaNO$_3$-rich particles, NaCl is nucleated homogeneously to crystallize in the core at
528   the single observed ERHs, whereas the NaNO$_3$ precipitate simultaneously on this core within the
529   time scale of the measurements. Although the NaNO$_3$-rich droplet was supersaturated with
530   NaNO$_3$ with decreasing RH during the dehydration process, NaNO$_3$ could not crystallize easily
531   even at the MERH of the NaCl-rich mixtures. Therefore, RHs lower than MERH (see Fig. 4 for
532   the lower ERHs in case of X_{NaCl} ≤ 0.3 than MERH) were necessary for the homogeneous
533   crystallization of NaCl followed by the almost simultaneous, induced heterogeneous
534   crystallization of NaNO$_3$.

535   Up until now, the binary inorganic salt aerosols, except the eutonic composition, are
536   generally believed to form a core-shell type heterogeneous solid of a pure salt core surrounded
537   by the eutonic component. The formation of the core-shell type had been reported for a range of
538   binary mixed aerosol particles, such as NaCl-KCl, KCl-KI, (NH$_4$)$_2$SO$_4$-NH$_4$NO$_3$ system (Ge et
539   al., 1996). Based on the secondary electron yield measurements of the NaCl-NaNO$_3$ mixture

540   particles, it was claimed that individual particles exist in core-shell form with the richer salt

541   (NaCl in NaCl-rich or $NaNO_3$ in $NaNO_3$-rich), and the eutonic components occupy the core and

542   shell, respectively (Ziemann and McMurry, 1997). However, the study was conducted on

543   particles nebulized from aqueous solutions that had not gone through the proper dehydration

544   process. Hoffmann et al. (2004) predicted a core-shell type structure based on their observations

545   of NaCl inclusions in the partially deliquesced particles only. On the other hand, a previous

546   report on NaCl-KCl mixture particles showed that NaCl and KCl were crystallized as separate

547   phases and not necessarily in the core-shell configuration. In addition, a eutonic solid shell in the

548   dry particle was found to be unnecessary for the exhibition of the two stage deliquescence

549   transitions during the humidifying process at all mixing ratios. The efflorescence phase diagram

550   (Fig. 4) and the X-ray maps (Fig. 5) showed that effloresced $NaCl$-$NaNO_3$ particles of all mixing

551   ratios had NaCl crystallized homogeneously in the center, surrounded either by the eutonic

552   component for $X_{NaCl} > 0.38$ or $NaNO_3$ for $X_{NaCl} \leq 0.38$. These micro-structures and spatial

553   distributions of chemical components have obvious atmospheric implications (Ziemann and

554   McMurry, 1997).

555

556   **4. Atmospheric implications**

557   The particle/droplet size variations with RH for the different mixing states (Fig. 2), the

558   four and three distinct phases observed during the humidifying (Fig. 3) and dehydration (Fig. 4)

559   processes, respectively, have important atmospheric implications in terms of radiative forcing

560   (Baynard et al., 2006; Ma et al., 2008), cloud nucleation efficiency (Petters et al., 2007; Wex et

561   al., 2008), atmospheric chemistry (Ault et al., 2013a; Ryder et al., 2014, Wang and Laskin, 2014),

562   and gas adsorption/desorption (gas-particle partitioning) (Woods et al., 2012). Some of these

563   implications related to the observed experimental results are discussed.

564

565   **4.1 Particle size change at different phase transitions**

566   In this study, the measured $NaCl$-$NaNO_3$ mixture particles, $1-10$ μm in size and their

567   size variations according to the RH change, are atmospherically relevant because inorganics are

568   dominant in the super-micron or coarse size fraction of SSAs (Keene et al., 2007; Ault et al.,

569   2013b; Prather et al., 2013). In Fig. 6A, 2D diameter ratios ($d/d_x = \sqrt{(A/A_x)}$, where x is the

570 particle state at RHs before the transitions), which represent the size increase due to mutual
571 deliquescence of the eutonic part at MDRH (compared to the rearranged solid particle) as well as
572 to deliquescence of the pure salts at the second DRHs (compared to the partially deliquesced

573 particle at MDRH), were plotted as a function of the NaCl mole fractions. As shown in Figs. 2
574 and 6A, the particle size variations during the humidifying process depends on the mixing ratio
575 of the two-component NaCl-NaNO$_3$ particles as the extent of the increase in particle size due to
576 the water uptake is associated with the chemical composition of the particles. For single-
577 component NaCl and NaNO$_3$ particles, their 2D diameters increase ~ 2.0 and ~ 1.5 fold,
578 respectively, when they deliquesced at their DRHs (Fig. 6A). The difference was attributed to the
579 different solubility of the salts. Because NaCl is less soluble than NaNO$_3$ (their solubility is
580 36.0g/100g and 91.2g/100g, respectively) (Lide, 2002), NaCl requires more water than NaNO$_3$ to
581 form a saturated solution, resulting in a larger increase in size when solid NaCl particles
582 deliquesce. Therefore, for the mixed NaCl-NaNO$_3$ particles, the extent of the particle size
583 increases at the MDRH or the second DRH is associated with the mixing ratios of the two salts.
584 At the MDRH, where only the eutonic component deliquesces, the extent of the size increase
585 depends on the fraction of the eutonic component in the particles. Therefore, at the MDRH,
586 particles with a eutonic composition (X_{NaCl} = 0.38) show the largest increase in size (d/d$_x$ = ~1.7
587 as shown in Fig. 6A). For NaCl-rich particles (X_{NaCl} > 0.38), the size increase at the MDRH
588 decreases with increasing NaCl fraction (Figs. 2d-f and 6A) because the eutonic fraction, which
589 depends on the NaNO$_3$ content in the particle, decreases with increasing NaCl mole fraction. In
590 contrast, for NaNO$_3$-rich particles (X_{NaCl} < 0.38), the size at the MDRH increases with increasing
591 NaCl fraction (Figs. 2a, 2b, and 6A), because the eutonic fraction, which depends on the NaCl
592 content, increases with increasing NaCl mole fraction. The particle size change at the RHs
593 between MDRH and the second DRH during the humidifying process depends on the residual
594 solid components after the mutual deliquescence. For NaCl-rich particles, the particles with a
595 larger NaCl fraction grow more at the RHs between MDRH and their second DRHs (Figs. 2d-f
596 and 6A) because the partially deliquesced particles have a larger residual NaCl solid fraction. In
597 contrast, for the NaNO$_3$-rich particles, the particles with the larger NaCl fraction grow less (Figs.
598 2a, 2b, and 6A), because they have a smaller residual NaCl solid fraction.
599 At the first ERH, where efflorescence occurs by the homogeneous nucleation of NaCl,
600 the NaCl-rich and eutonic droplets (X_{NaCl} ≥ 0.38) show a larger decrease in size for droplets of a

larger NaCl fraction (Fig. 6B). For the $NaNO_3$-rich droplets, the simultaneous heterogeneous precipitation of the $NaNO_3$ on the homogeneously-crystallized NaCl seeds occurs at their ERH, and the droplets of higher $NaNO_3$ content show a larger decrease in size. The decrease in size at the second efflorescence transition for aerosol particles of $X_{NaCl} \geq 0.38$ should be governed by the eutonic content in the aerosol particles; i.e., the more eutonic content, the greater the size decrease (Fig. 6B).

Aerosol particles with mixing ratios of $X_{NaCl} \geq 0.38$ did not show a noticeable change in the 2-D area when the RH was decreased from their first ERH to the start of the second ERH (MERH) (see Figs. 1g-i and 2c-f). At this RH range, the aerosol particles are expected to gradually decrease in size due to the evaporation of water in the eutonic solution. As discussed above, however, less soluble NaCl solid particles require more water than $NaNO_3$ to form a saturated solution, resulting in a larger increase in size when NaCl particles deliquesce (Fig. 6A). On the other hand, when aqueous NaCl droplets crystallize, more water in the droplets evaporates than when $NaNO_3$ is present in the droplets. For NaCl-rich droplets, because a large portion of water in the droplet might be removed when NaCl crystallizes at their first ERH, only a small amount of water remains in the eutonic solution, which evaporates gradually until complete efflorescence occurs, even though shrinkage was not observed well on their optical images. On the other hand, in this RH range, the particle boundary appeared to be clearer when it became more concentrated with decreasing RH. Indeed, the change was clear when viewed directly through the optical microscope (unlike the digital images) during the dehydration measurements. The size variations of aerosol particles with different mixing ratios according to the RH change can help predict their aerodynamic properties and hence their residence time in ambient air. These variations, however, also depend on the original size of the particles, possibly more for sub-micron particles (Hu et al., 2010).

4.2 Hygroscopic growth and cloud droplet nucleation

Cloud droplet nucleation can begin when the air is supersaturated with water vapor (i.e., RH is above 100%) and the hygroscopic growth at high RHs are correlated with the cloud condensation nuclei (CCN) activity (Petters et al., 2007; Wex et al., 2008). Under these experimental conditions, the highest working RH was ~ 93%. On the other hand, as the DRHs of

23

632   pure NaCl and NaNO$_3$ are 75.5($\pm$0.5)% and 74.0($\pm$0.5)%, respectively, the hygroscopic growth

633   begins at less than ~76% RH for particles of all mixing ratios. In Fig. 7, the growth factors in

634   terms of the 2D diameter ratios (d$_{95}$/d$_0$, where d$_{95}$ $\equiv$ the diameter at RH = 95%, determined by

635   extrapolation, and d$_0$ $\equiv$ dry diameter at ~3% RH) are plotted as a function of the mole fraction of

636   NaCl for the NaCl-NaNO$_3$ mixture particles to indicate the cloud droplet nucleation efficiency of

637   these particles at various mixing ratios. NaCl, eutonic, and NaNO$_3$ particles, which have single

638   deliquescence transitions (one DRH), appear to show relatively higher hygroscopic growth, in

639   the order, NaCl > eutonic > NaNO$_3$, than particles with other mixing ratios, having two-stage

640   deliquescence (MDRH and the second DRH). The hygroscopic growth first decreases with

641   decreasing eutonic content for NaCl-rich particles with $0.38 < X_{NaCl} \leq 0.6$ and then begins to

642   increase with increasing NaCl content for particles with $0.6 < X_{NaCl} \leq 1.0$. Similar behavior was

643   observed for NaNO$_3$-rich particles. Therefore, for NaCl-NaNO$_3$ mixture particles, the CCN

644   efficiency should also follow the same trend. This can serve as a precursor to the hygroscopic

645   growth and CCN activity of more complex, reacted SSAs containing other salts and organics

646   (King et al., 2012). However, an estimation of the full CCN activity and cloud droplet number

647   concentration require further experiments on a wider dry particle size range under both under-

648   and super-saturated conditions (Fuentes et al., 2011; Mochida et al., 2011).

649

650   **4.3 Atmospheric chemistry**

651   The knowledge of mixing states, phases, and spatial distribution of chemicals of NaCl-

652   NaNO$_3$ mixture particles, as reacted SSA surrogates, at various RHs is expected to help better

653   understand the complexity of real ambient SSAs, their hygroscopic properties, aqueous phase

654   chemistry, etc. For SSAs comprising NaCl-NaNO$_3$ mixture particles generated from a partial or

655   full reaction with NO$_x$/HNO$_3$, their aqueous surface regions are crucial for atmospheric

656   heterogeneous chemistry because the aqueous phases of NaCl, NaNO$_3$, or the eutonic composed

657   part at different RHs are expected to be available for further reactions with gas phase species,

658   such as N$_2$O$_5$ (Ault et al., 2013a; Ryder et al., 2014) or organics (Wang and Laskin, 2014), and/or

659   for facile gas-particle partitioning (Woods et al., 2012).

660   SSAs are generated by sea-spray action, so that they are initially aqueous droplets when

661   they become airborne. Although real ambient SSAs are complex mixtures containing NaCl, other

24

inorganic salts, and organics (O'Dowd and de Leeuw, 2007; Keene et al., 2007; Prather et al., 2013; Beardsley et al., 2013; Ault et al., 2013b), NaCl particles have been studied as genuine SSA surrogates in many laboratories (Martin, 2000; Krieger et al., 2012). Based on the experimental phase diagrams of deliquescence and efflorescence for the NaCl and NaNO$_3$ system (Figs. 3 and 4), once airborne as droplets, the genuine SSA surrogate would remain in the aqueous phase unless the droplets experience an ambient RH below their ERH of 47.6 − 46.3% (pure NaCl). Their aqueous phase can facilitate heterogeneous reactions with gaseous species, such as NO$_x$/HNO$_3$, to become NaCl-NaNO$_3$ mixture droplets. When mixture droplets are formed, their full efflorescence occurs at lower RHs (i.e., at MERH of ~33.1% for the mixture droplets of $X_{NaCl} \geq 0.38$ or at ERH of ~35-21% for those of $X_{NaCl} < 0.38$; see Fig. 4) than ERH for pure NaCl, so that their chance for a further gas-particle interaction would be larger with less probability to fully effloresce. Even when the mixed particles become solids due to the full efflorescence below either their MDRH or ERH, they can deliquesce at a lower DRH (i.e., the NaCl-NaNO$_3$ mixed particles with various mixing ratios partially deliquesce at a MDRH of ~67.9%, whereas pure NaCl deliquesces at a DRH of ~75.5%; see Fig. 3). In other words, NaCl-NaNO$_3$ mixture aerosol particles can maintain an aqueous phase over a wider RH range than the genuine SSA surrogate, making their heterogeneous chemistry more probable. Therefore, NaCl-rich particles with higher Cl$^-$/NO$_3^-$ can show higher uptake of N$_2$O$_5$ at ambient RHs (usually > 60%) in the marine boundary layer (Ryder et al., 2014). On the other hand, a high uptake of HNO$_3$ due to surface adsorbed moisture on crystalline NaCl particles has also been reported (Saul et al., 2006; Liu et al., 2007). The ionic activities of aqueous Na$^+$/Cl$^-$/NO$_3^-$ at high to very low water activities during hydration and dehydration, indicating the chemical reactivity of these ions, can be calculated using the AIOMFAC model.

5. Conclusion

The hygroscopic behavior and microstructures of mixed NaCl-NaNO$_3$ particles at various mixing ratios collected on a TEM grid were investigated by the use of optical microscopy and SEM/EDX. The DRHs and ERHs of the mixed NaCl-NaNO$_3$ particles in the micrometer size range at room temperature were determined by monitoring the change in the particle area in 2D optical images with the RH variation of ~ 3−93%. During the humidifying

process, the particles with a eutonic composition (X_{NaCl} = 0.38) exhibited single-stage deliquescence behavior at MDRH = 67.9($\pm$ 0.5)%. The mixed NaCl-NaNO$_3$ particles, except for the eutonic composition, showed two-stage phase transitions: the first transition at MDRH, which is independent of the chemical compositions, and the second transition at the DRHs, which depend on the mixing ratios of the two salts. For the NaCl-rich particles (X_{NaCl} > 0.38), the increase in the mole fraction of NaCl shifted the DRH toward a pure NaCl limit (DRH = 75.5($\pm$0.5)%). For NaNO$_3$-rich particles (X_{NaCl} < 0.38), the increase in the mole fraction of NaNO$_3$ shifted the DRH toward the pure NaNO$_3$ limit (DRH = 74.0($\pm$0.5)%). The measured DRH values agreed well with those calculated from the thermodynamic AIOMFAC model.

The dehydration behavior of the mixed NaCl-NaNO$_3$ particles depend on the mixing ratios of the two salts. NaCl-rich particles (X_{NaCl} > 0.38) showed two-stage efflorescence transitions: the first stage, which is driven purely by the homogeneous nucleation of NaCl, and the second stage at MERH. Interestingly, the eutonic composed particles (X_{NaCl} = 0.38) also showed two stage efflorescence with NaCl crystallizing first followed by the heterogeneous nucleation of NaNO$_3$ on NaCl seeds. NaNO$_3$-rich particles (X_{NaCl} $\leq$ 0.3) showed single-stage efflorescence transitions at ERHs progressively lower than MERH due to the slower homogeneous nucleation of NaCl and the simultaneous heterogeneous efflorescence of NaNO$_3$ on the NaCl seeds. SEM/EDX elemental mapping shows that effloresced NaCl-NaNO$_3$ particles of all mixing ratios had NaCl crystallized homogeneously in the center, surrounded either by the eutonic component for X_{NaCl} > 0.38 or NaNO$_3$ for X_{NaCl} $\leq$ 0.38. A pure salt core and eutonic composed solid shell in the dry particle was not necessary for exhibiting the two stage deliquescence transitions in all mixing ratios.

During humidifying or dehydration processes, the amount of the eutonic composed part drives the particle/droplet growth or shrinkage at the MDRH or MERH (second ERH), respectively, and the amount of ~~remnant~~ pure salts (NaCl or NaNO$_3$ in NaCl- or NaNO$_3$-rich particles, respectively) does at the second DRHs or first ERHs, respectively. Therefore, their behavior can be a precursor to the optical properties and direct radiative forcing for these atmospherically relevant mixture particles representing the coarse, reacted inorganic SSAs. On the other hand, the hygroscopic growth at a RH of 95% for the various mixing ratios of these mixture particles can be a precursor to the cloud droplet nucleation efficiency and indirect

서식 있음: 취소선

radiative forcing. In addition, NaCl-NaNO$_3$ mixture aerosol particles can maintain an aqueous phase over a wider RH range than the genuine SSA surrogate (i.e., pure NaCl particles), making their heterogeneous chemistry more likely.

References

Ahn, K.-H., Kim, S.-M., Jung, H.-J., Lee, M.-J., Eom, H.-J., Maskey, S., and Ro, C.-U.: Combined use of optical and electron microscopic techniques for the measurement of hygroscopic property, chemical composition, and morphology of individual aerosol particles, Anal. Chem., 82, 7999-8009, 2010.

Ansari, A. S., and Pandis, S. N.: Prediction of multicomponent inorganic atmospheric aerosol behavior, Atmos. Environ., 33, 745-757, 1999.

Ault, A. P., Guasco, T. L., Ryder, O. S., Baltrusaitis, J., Cuadra-Rodriguez, L. A., Collins, D. B., Ruppel, M. J., Bertram, T. H., Prather, K. A., and Grassian, V. H.: Inside versus Outside: Ion Redistribution in Nitric Acid Reacted Sea Spray Aerosol Particles as Determined by Single Particle Analysis, J. Am. Chem. Soc., 135, 14528-14531, 10.1021/ja407117x, 2013a.

Ault, A. P., Moffet, R. C., Baltrusaitis, J., Collins, D. B., Ruppel, M. J., Cuadra-Rodriguez, L. A., Zhao, D., Guasco, T. L., Ebben, C. J., Geiger, F. M., Bertram, T. H., Prather, K. A., and Grassian, V. H.: Size-Dependent Changes in Sea Spray Aerosol Composition and Properties with Different Seawater Conditions, Environ. Sci. Technol., 47, 5603-5612, 10.1021/es400416g, 2013b.

Ault, A. P., Guasco, T. L., Baltrusaitis, J., Ryder, O. S., Trueblood, J. V., Collins, D. B., Ruppel, M. J., Cuadra-Rodriguez, L. A., Prather, K. A., and Grassian, V. H.: Heterogeneous Reactivity of Nitric Acid with Nascent Sea Spray Aerosol: Large Differences Observed between and within Individual Particles, J. Phys. Chem. Lett., 5, 2493-2500, 10.1021/jz5008802, 2014.

Baynard, T., Garland, R. M., Ravishankara, A. R., Tolbert, M. A., and Lovejoy, E. R.: Key factors influencing the relative humidity dependence of aerosol light scattering, Geophys. Res. Lett., 33, L06813, 10.1029/2005gl024898, 2006.

Beardsley, R., Jang, M., Ori, B., Im, Y., Delcomyn, C. A., and Witherspoon, N.: Role of sea salt

aerosols in the formation of aromatic secondary organic aerosol: yields and hygroscopic properties, Environmental Chemistry, 10, 167-177, http://dx.doi.org/10.1071/EN13016, 2013.

Chang, S.-Y., and Lee C.-T.: Applying GC-TCD to investigate the hygroscopic characteristics of mixed aerosols, Atmos. Environ., 36, 1521–1530, 2002.

Clegg, S. L., Brimblecombe P., and Wexler, A. S.: A thermodynamic model of the system H^+ - NH_4^+ - Na^+ - SO_4^{2-} - NO_3^- - Cl^- - H_2O at 298.15 K, J. Phys. Chem. A 102, 2155-2171, 1998.

Cohen, M. D., Flagan, R. C., and Seinfeld, J. H.: Studies of concentrated electrolyte solutions using the electrodynamic balance. 2. Water activities for mixed-electrolyte solutions, J. Phys. Chem., 91, 4575-4582, 10.1021/j100301a030, 1987a.

Cohen, M. D., Flagan, R. C., and Seinfeld, J. H.: Studies of concentrated electrolyte solutions using the electrodynamic balance. 3. Solute nucleation, J. Phys. Chem., 91, 4583-4590, 10.1021/j100301a031, 1987b.

Eom, H.-J., Gupta, D., Li, X., Jung, H.-J., Kim, H., and Ro, C.-U.: Influence of Collecting Substrates on the Characterization of Hygroscopic Properties of Inorganic Aerosol Particles, Anal. Chem., 86, 2648-2656, 10.1021/ac4042075, 2014.

Finlayson-Pitts, B. J., and Pitts, J. N. J.: Chemistry of the upper and lower atmosphere theory, experiments, and applications, San Diego: Academic Press, 2000.

Freney, E. J., Martin, S. T., and Buseck, P. R.: Deliquescence and Efflorescence of Potassium Salts Relevant to Biomass-Burning Aerosol Particles, Aerosol Sci. and Technol., 43,799–807, 2009.

Freney, E. J., Adachi, K., and Buseck, P. R.: Internally mixed atmospheric aerosol particles: Hygroscopic growth and light scattering, J. Geophys. Res., 115, D19210, doi:10.1029/2009JD013558, 2010.

Fuentes, E., Coe, H., Green, D., and McFiggans, G.: On the impacts of phytoplankton-derived organic matter on the properties of the primary marine aerosol – Part 2: Composition, hygroscopicity and cloud condensation activity, Atmos. Chem. Phys., 11, 2585-2602, 10.5194/acp-11-2585-2011, 2011.

Gao, Y., Yu, L. E., and Chen, S. B.: Efflorescence Relative Humidity of Mixed Sodium Chloride and Sodium Sulfate Particles, J. Phys. Chem. A, 111, 10660-10666, 10.1021/jp073186y, 2007.

Gard, E. E., Kleeman, M. J., Gross, D. S., Hughes, L. S., Allen, J. O., Morrical, B. D., Fergenson, D. P., Dienes, T., Galli, M. E., Johnson, R. J., Cass, G. R., and Prather, K. A.: Direct Observation of Heterogeneous Chemistry in the Atmosphere Science, Science, 279, 1184- 1187, 1998.

Ge, Z., Wexler, A. S., and Johnston, M. V.: Multicomponent Aerosol Crystallization, J. Colloid Interface Sci., 183, 68–77, 1996.

809

810   Ge, Z., Wexler, A. S., and Johnston, M. V.: Deliquescence Behavior of Multicomponent Aerosols,
811   J. Phys. Chem. A, 102, 173–180, 1998.

812

813   Gibson, E. R., Hudson, P. K., and Grassian, V. H.: Physicochemical Properties of Nitrate
814   Aerosols: Implications for the Atmosphere, J. Phys. Chem. A, 110, 11785-11799,
815   10.1021/jp063821k, 2006.

816

817   Gysel, M., Weingartner, E., and Baltensperger, U.: Hygroscopicity of aerosol particles at low
818   temperatures. 2. Theoretical and experimental hygroscopic properties of laboratory generated
819   aerosols. Environ. Sci. Technol., 36, 63-68, doi:10.1021/es010055g, 2002.

820

821   Haywood, J., and Boucher, O.: Estimates of the direct and indirect radiative forcing due to
822   tropospheric aerosols: A review, Rev. Geophys., 38, 513-543, 10.1029/1999rg000078, 2000.

823

824   Hoffman, R. C., Laskin, A., and Finlayson-Pitts, B. J.: Sodium nitrate particles: physical and
825   chemical properties during hydration and dehydration, and implications for aged sea salt aerosols,
826   J. of Aerosol Sci., 35, 869–887, 2004.

827

828   Hu, D., Qiao, L., Chen, J., Ye, X., Yang, X., Cheng, T., and Fang, W.: Hygroscopicity of
829   Inorganic Aerosols: Size and Relative Humidity Effects on the Growth Factor, Aerosol Air Qual.
830   Res., 10, 255-264, 10.4209/aaqr.2009.12.0076, 2010.

831

832   Keene, W. C., Maring, H., Maben, J. R., Kieber, D. J., Pszenny, A. A. P., Dahl, E. E., Izaguirre,
833   M. A., Davis, A. J., Long, M. S., Zhou, X., Smoydzin, L., and Sander, R.: Chemical and physical
834   characteristics of nascent aerosols produced by bursting bubbles at a model air-sea interface, J.
835   Geophys. Res. — Atmos., 112, D21202, 10.1029/2007jd008464, 2007.

836

837   Kelly J. T., Wexler A. S. Chan C. K., and Chan M. N.: Aerosol thermodynamics of potassium
838   salts, double salts, and water content near the eutectic, Atmos. Environ. 42, 3717-3728, 2008.

839

840   Kim, H. -K., Lee, M.-J., Jung, H.-J., Eom, H.-J. Maskey, S., Ahn, K.-H., and Ro, C.-U.:
841   Hygroscopic behavior of wet dispersed and dry deposited $NaNO_3$ particles, Atmos. Environ., 60,
842   68-75, 2012.

843

844   King, S. M., Butcher, A. C., Rosenoern, T., Coz, E., Lieke, K. I., de Leeuw, G., Nilsson, E. D.,
845   and Bilde, M.: Investigating Primary Marine Aerosol Properties: CCN Activity of Sea Salt and
846   Mixed Inorganic–Organic Particles, Environ. Sci. Technol., 46, 10405-10412,
847   10.1021/es300574u, 2012.

848

849   Krieger, U. K., Marcolli, C., and Reid, J. P.: Exploring the complexity of aerosol particle
850   properties and processes using single particle techniques, Chem. Soc. Rev., 41, 6631-6662,
851   10.1039/c2cs35082c, 2012.

852

853   Krueger, B. J., Grassian, V. H., Iedema, M. J., Cowin, J. P., and Laskin, A.: Probing
854   Heterogeneous Chemistry of Individual Atmospheric Particles Using Scanning Electron

Microscopy and Energy-Dispersive X-ray Analysis, Anal. Chem., 75, 5170-5179, 10.1021/ac034455t, 2003.

Laskin, A., Gaspar, D. J., Wang, W., Hunt, S. W., Cowin, J. P., Colson, S. D., and Finlayson-Pitts, B. J.: Reactions at Interfaces As a Source of Sulfate Formation in Sea-Salt Particles, Science, 301, 340-344, 10.1126/science.1085374, 2003.

Lee C. -T., and Hsu, W. -C.: The Measurement of Liquid Water Mass Associated with Collected Hygroscopic Particles, J. Aerosol Sci., 31, 189-197, 2000.

Li, X., Gupta, D., Eom, H.-J., Kim, H., and Ro, C.-U.: Deliquescence and efflorescence behavior of individual NaCl and KCl mixture aerosol particles, Atmos. Environ., 82, 36-43, 10.1016/j.atmosenv.2013.10.011, 2014.

Lide, D. R.: Handbook of Chemistry and Physics Eighty third ed., edited by: Lide, D. R., CRC Press, Boca Raton, Florida, 2002.

Liu, Y., Cain, J. P., Wang, H., and Laskin, A.: Kinetic Study of Heterogeneous Reaction of Deliquesced NaCl Particles with Gaseous HNO_3 Using Particle-on-Substrate Stagnation Flow Reactor Approach, J. Phys. Chem. A, 111, 10026-10043, 10.1021/jp072005p, 2007.

Ma, X., von Salzen, K., and Li, J.: Modelling sea salt aerosol and its direct and indirect effects on climate, Atmos. Chem. Phys., 8, 1311-1327, 10.5194/acp-8-1311-2008, 2008.

Martin, S. T.: Phase Transitions of Aqueous Atmospheric Particles, Chem. Rev., 100, 3403-3453, 2000.

McInnes, L.M., Quinn, P.K., Covert, D.S., and Anderson, T.L.: Gravimetric analysis, ionic composition, and associated water mass of the marine aerosol, Atmos. Environ., 30, 869-884, 1996.

Meskhidze, N., Petters, M. D., Tsigaridis, K., Bates, T., O'Dowd, C., Reid, J., Lewis, E. R., Gantt, B., Anguelova, M. D., Bhave, P. V., Bird, J., Callaghan, A. H., Ceburnis, D., Chang, R., Clarke, A., de Leeuw, G., Deane, G., DeMott, P. J., Elliot, S., Facchini, M. C., Fairall, C. W., Hawkins, L., Hu, Y., Hudson, J. G., Johnson, M. S., Kaku, K. C., Keene, W. C., Kieber, D. J., Long, M. S., Mårtensson, M., Modini, R. L., Osburn, C. L., Prather, K. A., Pszenny, A., Rinaldi, M., Russell, L. M., Salter, M., Sayer, A. M., Smirnov, A., Suda, S. R., Toth, T. D., Worsnop, D. R., Wozniak, A., and Zorn, S. R.: Production mechanisms, number concentration, size distribution, chemical composition, and optical properties of sea spray aerosols, Atmospheric Science Letters, 14, 207-213, 10.1002/asl2.441, 2013.

Mikhailov, E., Vlasenko, S., Martin, S. T., Koop, T., and Pöschl, U.: Amorphous and crystalline aerosol particles interacting with water vapor: conceptual framework and experimental evidence for restructuring, phase transitions and kinetic limitations, Atmos. Chem. Phys., 9, 9491–9522, doi:10.5194/acp-9-9491-2009, 2009.

Mochida, M., Nishita-Hara, C., Furutani, H., Miyazaki, Y., Jung, J., Kawamura, K., and Uematsu, M.: Hygroscopicity and cloud condensation nucleus activity of marine aerosol particles over the western North Pacific, J. Geophys. Res. — Atmos., 116, D06204, 10.1029/2010jd014759, 2011.

O'Dowd, C. D., and de Leeuw, G.: Marine aerosol production: a review of the current knowledge, Philosophical Transactions of the Royal Society A: Mathematical, Physical and Engineering Sciences, 365, 1753-1774, 10.1098/rsta.2007.2043, 2007.

Pandis, S. N., Wexler, A. S., and Seinfeld, J. H.: Dynamics of tropospheric aerosols (Review). J. Phys. Chem., 99, 9646–9659, 1995.

Petters, M. D., and Kreidenweis, S. M.: A single parameter representation of hygroscopic growth and cloud condensation nucleus activity, Atmos. Chem. Phys., 7, 1961-1971, 10.5194/acp-7-1961-2007, 2007.

Prather, K. A., Bertram, T. H., Grassian, V. H., Deane, G. B., Stokes, M. D., DeMott, P. J., Aluwihare, L. I., Palenik, B. P., Azam, F., Seinfeld, J. H., Moffet, R. C., Molina, M. J., Cappa, C. D., Geiger, F. M., Roberts, G. C., Russell, L. M., Ault, A. P., Baltrusaitis, J., Collins, D. B., Corrigan, C. E., Cuadra-Rodriguez, L. A., Ebben, C. J., Forestieri, S. D., Guasco, T. L., Hersey, S. P., Kim, M. J., Lambert, W. F., Modini, R. L., Mui, W., Pedler, B. E., Ruppel, M. J., Ryder, O. S., Schoepp, N. G., Sullivan, R. C., and Zhao, D.: Bringing the ocean into the laboratory to probe the chemical complexity of sea spray aerosol, Proceedings of the National Academy of Sciences, 110, 7550-7555, 10.1073/pnas.1300262110, 2013.

Ro, C.-U., Oh, K.-Y., Kim, H., Kim, Y. P., Lee, C. B., Kim, K.-H., Osan, J., de Hoog, J., Worobiec, A., and Van Grieken, R.: Single Particle Analysis of Aerosols at Cheju Island, Korea, Using Low-Z Electron Probe X-ray Microanalysis: A Direct Proof of Nitrate Formation from Sea-Salts, Environ. Sci. Technol., 35, 4487-4494, 2001.

Ryder, O. S., Ault, A. P., Cahill, J. F., Guasco, T. L., Riedel, T. P., Cuadra-Rodriguez, L. A., Gaston, C. J., Fitzgerald, E., Lee, C., Prather, K. A., and Bertram, T. H.: On the Role of Particle Inorganic Mixing State in the Reactive Uptake of N_2O_5 to Ambient Aerosol Particles, Environ. Sci. Technol., 48, 1618-1627, 10.1021/es4042622, 2014.

Satheesh, S. K., and Moorthy, K. K.: Radiative effects of natural aerosols: A review, Atmos. Environ., 39, 2089-2110, 2005.

Saul, T. D., Tolocka, M. P., and Johnston, M. V.: Reactive Uptake of Nitric Acid onto Sodium Chloride Aerosols Across a Wide Range of Relative Humidities, J. Phys. Chem. A, 110, 7614-7620, 10.1021/jp060639a, 2006.

Schlenker, J. C., and Martin, S. T.: Crystallization Pathways of Sulfate-Nitrate-Ammonium Aerosol Particles, J. Phys. Chem. A, 109, 9980–9985, 2005.

Seinfeld, J. H., and Pandis, S. N.: Atmospheric chemistry and physics : from air pollution to climate change, 2nd ed., J. Wiley, Hoboken, N.J., xxviii, 1203 p. pp., 2006.

947

948 Tang, I. N.: Phase Transformation and Growth of Aerosol Particles Composed of Mixed Salts, J.
949 Aerosol Sci., 7, 361-371, 1976.

950

951 Tang, I. N., and Munkelwitz, H. R.: Composition and temperature dependence of the
952 deliquescence properties of hygroscopic aerosols, Atmos. Environ. 27A, 467-473, 1993.

953

954 Tang, I. N., and Munkelwitz, H. R.: Aerosol Phase Transformation and Growth in the
955 Atmosphere, J. Appl. Meteorol., 33, 791–796, 1994a.

956

957 Tang, I. N., and Munkelwitz, H. R.: Water activities, densities, and refractive indices of aqueous
958 sulfates and sodium nitrate droplets of atmospheric importance, J. Geophys. Res., 99 18801-
959 18808, 1994b.

960

961 Tang, I. N., Munkelwitz, H. R., and Davis, J. G.: Aerosol Growth Studies – IV Phase
962 Transformation of Mixed Salt Aerosols in a Moist Atmosphere, J. Aerosol Sci., 9, 505-511, 1978.

963

964 Tang, I. N., Tridico, A. C., and Fung, K. H.: Thermodynamics and optical properties of sea salt
965 aerosols, J. Geophys. Res., 102, 23269-23275, 1997.

966

967 ten Brink, H. M.: Reactive uptake of HNO_3 and H_2SO_4 in sea-salt (NaCl) particles, J. Aerosol
968 Sci., 29, 57-64, http://dx.doi.org/10.1016/S0021-8502(97)00460-6, 1998.

969

970 Wang, B., and Laskin, A.: Reactions between water-soluble organic acids and nitrates in
971 atmospheric aerosols: Recycling of nitric acid and formation of organic salts, J. Geophys. Res. -
972 Atmos., 119, 2013JD021169, 10.1002/2013jd021169, 2014.

973

974 Wang, J., and Martin, S. T.: Satellite characterization of urban aerosols: Importance of including
975 hygroscopicity and mixing state in the retrieval algorithms, J. Geophys. Res. — Atmos., 112,
976 D17203, 10.1029/2006jd008078, 2007.

977

978 Wex, H., Stratmann, F., Hennig, T., Hartmann, S., Niedermeier, D., Nilsson, E., Ocskay, R., Rose,
979 D., Salma, I., and Ziese, M.: Connecting hygroscopic growth at high humidities to cloud
980 activation for different particle types, Environ. Res. Lett., 3, 035004, 2008.

981

982 Wexler, A. S., and Clegg, S. L.: Atmospheric aerosol models for systems including the ions H^+,
983 NH_4^+, Na^+, SO_4^{2-}, NO_3^-, Cl^-, Br^-, and H_2O, J. Geophys. Res., Vol.107, No. D14, 4207,
984 10.1029/2001JD000451, 2002.

985

986 Wexler, A. S., and Seinfeld J. H.: Second-generation inorganic aerosol model, Atmos. Environ.
987 25A, 2731-2748, 1991.

988

989 Wise, M. E., Semeniuk, T. A., Bruintjes, R., Martin, S. T., Russell, L. M., and Buseck, P. R.:
990 Hygroscopic behavior of NaCl-bearing natural aerosol particles using environmental
991 transmission electron microscopy, J. Geophys. Res., 112, D10224, doi:10.1029/2006JD007678,
992 2007.

993
994 Wise, M. E., Freney, E. J., Tyree, C. A., Allen, J. O., Martin S. T., Russell L. M., and Buseck P.
995 R.: Hygroscopic behavior and liquid-layer composition of aerosol particles generated from
996 natural and artificial seawater, J. Geophys. Res.114, D03201, doi:10.1029/2008JD010449, 2009.
997
998 Woods, E., Yi, C., Gerson, J. R., and Zaman, R. A.: Uptake of Pyrene by NaCl, NaNO$_3$, and
999 MgCl$_2$ Aerosol Particles, J. Phys. Chem. A, 116, 4137-4143, 10.1021/jp3014145, 2012.
1000
1001 Ziemann, P. J., and McMurry, P. H.: Spatial Distribution of Chemical Components in Aerosol
1002 Particles as Determined from Secondary Electron Yield Measurements: Implications for
1003 Mechanisms of Multicomponent Aerosol Crystallization, J. Colloid Interface Sci., 193, 250–258,
1004 1997.
1005
1006 Zuend, A., Marcolli, C., Luo, B. P., and Peter, T.: A thermodynamic model of mixed organic-
1007 inorganic aerosols to predict activity coefficients, Atmos. Chem. Phys., 8, 4559-4593,
1008 10.5194/acp-8-4559-2008, 2008.
1009
1010 Zuend, A., Marcolli, C., Booth, A. M., Lienhard, D. M., Soonsin, V., Krieger, U. K., Topping, D.
1011 O., McFiggans, G., Peter, T., and Seinfeld, J. H.: New and extended parameterization of the
1012 thermodynamic model AIOMFAC: calculation of activity coefficients for organic-inorganic
1013 mixtures containing carboxyl, hydroxyl, carbonyl, ether, ester, alkenyl, alkyl, and aromatic
1014 functional groups, Atmos. Chem. Phys., 11, 9155–9206, doi:10.5194/acp-11-9155-2011, 2011.

Figure 1. Optical images of NaCl-NaNO$_3$ particles with a mole fraction of $X_{NaCl} = 0.8$, obtained during humidifying (↑) and dehydration (↓) processes for the same image field.

(a) RH = 3.0%
(b) RH = 67.7%
(c) RH = 68.0% (MDRH)
(d) RH = 73.7% (2nd DRH)
(e) RH = 85.5%
(f) RH = 46.6%
(g) RH = 45.1% (1st ERH)
(h) RH = 32.5%
(i) RH = 32.2% (MERH)
(j) RH = 2.9 %
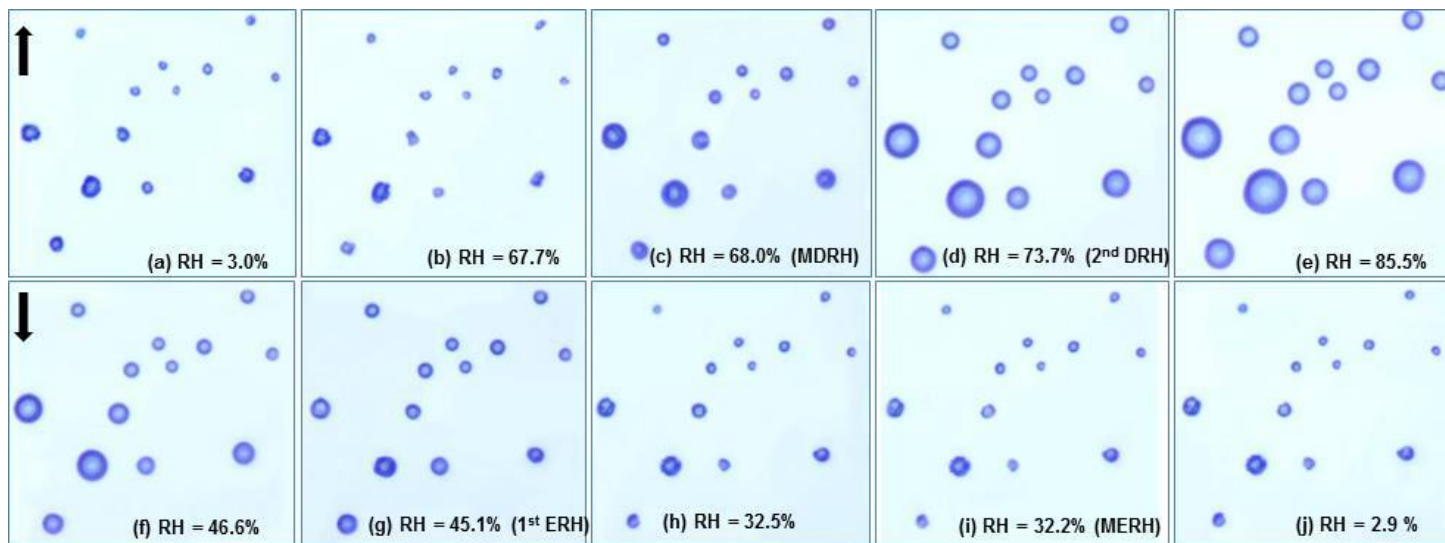
Figure 2. Plots of 2D projected area ratio as a function of the relative humidity (humidifying process: closed circles; dehydration process: open triangles) for different mole fractions of NaCl-NaNO$_3$, expressed in X_{NaCl} values of (a) 0.1 (NaNO$_3$-rich), (b) 0.2 (NaNO$_3$-rich), (c) 0.38 (eutonic), (d) 0.5 (equi-molar/NaCl-rich), (e) 0.8 (NaCl-rich), and (f) 0.9 (NaCl-rich). The transition relative humidity in both humidifying and dehydration processes are marked with arrows.
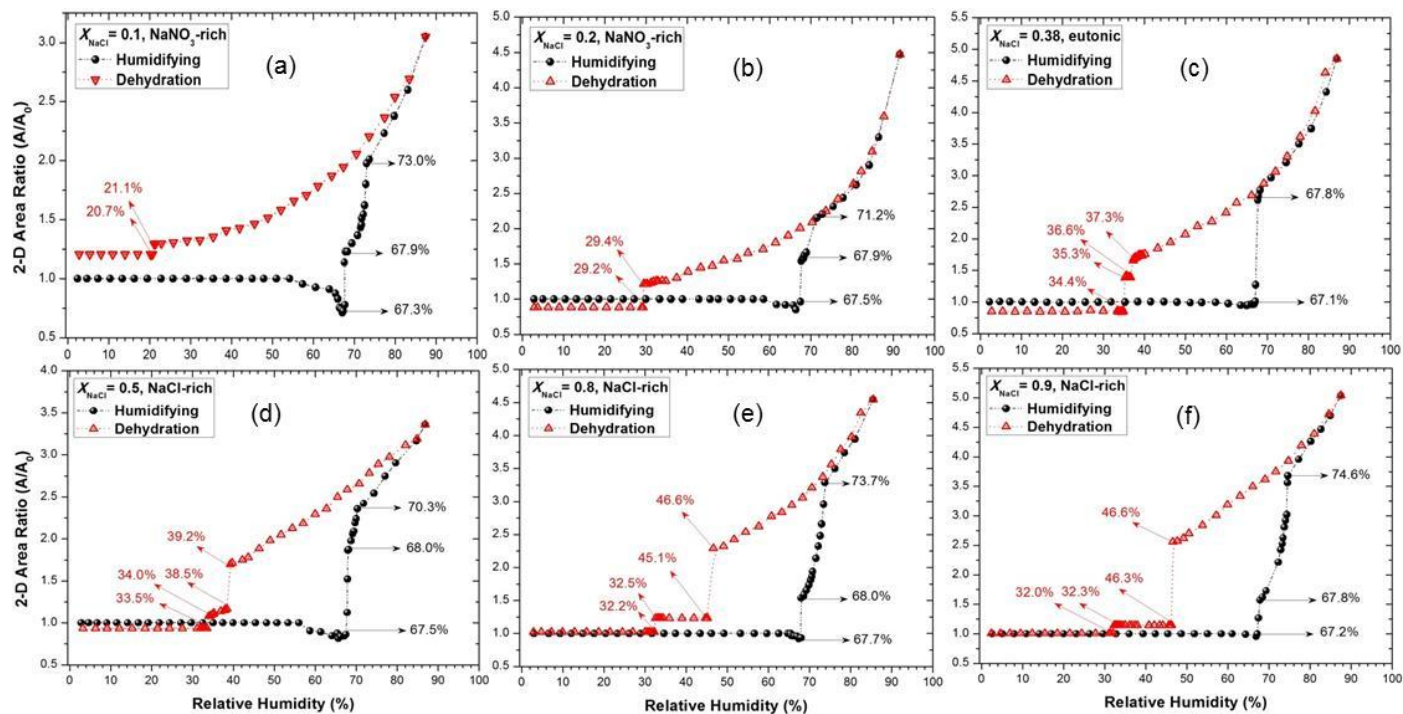
Figure 3. Measured first DRH or MDRH (open triangles), second DRH (closed circles) values, calculated MDRH (dotted line), and the second DRHs (dash-dotted curve) from the AIOMFAC, plotted as a function of the mole fraction of NaCl in NaCl-NaNO$_3$ mixture particles. The phase notations shown in brackets are s ≡ solid; and aq ≡ aqueous.
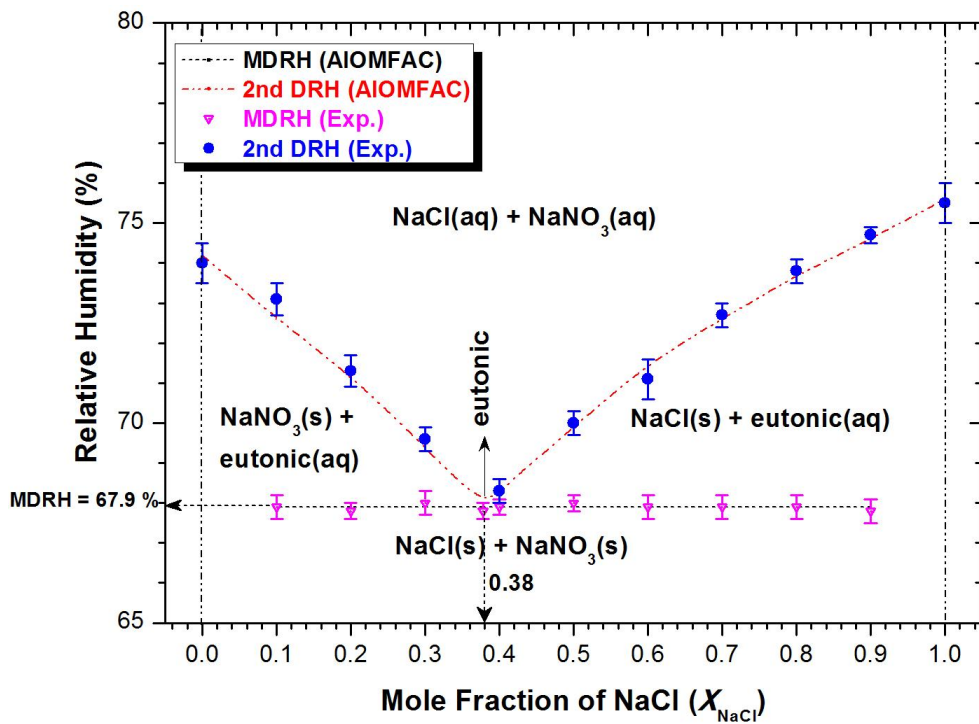
Figure 4. Measured first ERH values (open circles) and second ERH values (open triangles) as a function of the mole fraction of NaCl in NaCl-NaNO$_3$ mixture particles as well as ERH (closed circle) for wet deposited NaNO$_3$ particles containing seeds. The phase notations shown in brackets are s ≡ solid; and aq ≡ aqueous.
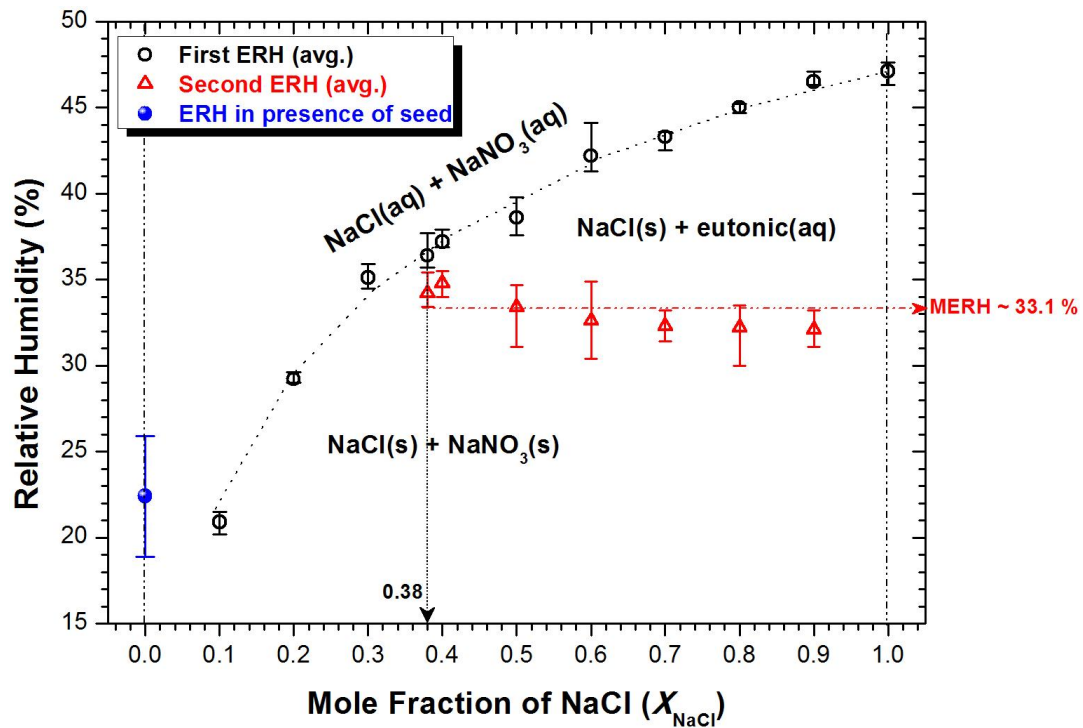
Figure 5. Secondary electron images (SEIs) and elemental X-Ray maps for Cl (from NaCl), O (from NaNO$_3$), and Na of the effloresced NaCl-NaNO$_3$ mixture particles with compositions of (a) $X_{NaCl} = 0.8$ (NaCl-rich); (b) $X_{NaCl} = 0.38$ (eutonic); and (c) $X_{NaCl} = 0.2$ (NaNO$_3$-rich).
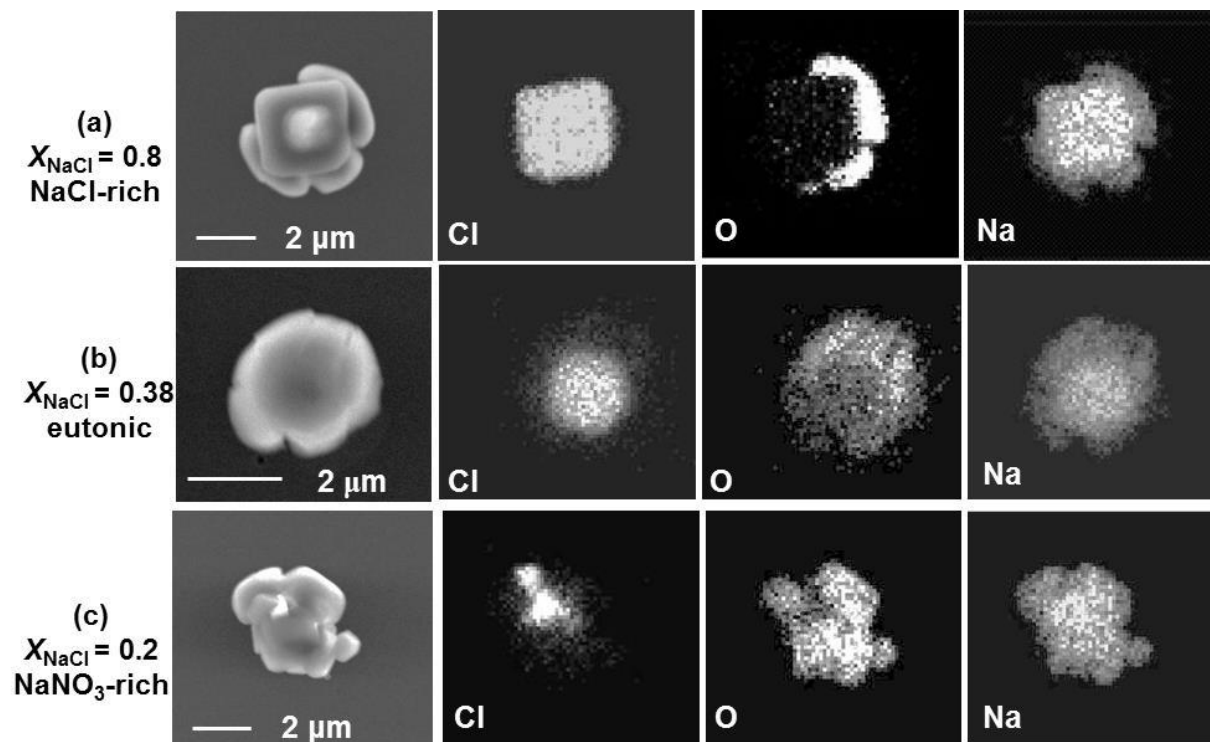
Figure 6. (A) 2D diameter ratios (d/d_x) of the particles/aerosols plotted as a function of the NaCl mole fractions (X_{NaCl}), which represent the size increase due to the mutual deliquescence of the eutonic part at MDRH ("d") compared to that of the solid particle at the start of the first transition ("d_x") (eutonic: open squares); and due to the complete deliquescence of the pure salts (in the figure, NaNO$_3$: closed circles and NaCl: open circles) at their second DRHs ("d") compared to that of the partially deliquesced particle at MDRH ("d_x") and (B) 2D diameter ratios (d/d_x) of droplets/aerosols plotted as a fucntion of the NaCl mole fractions (X_{NaCl}), which represent the size decrease due to the efflorescence of NaCl ("d") compared to that of the liquid droplets at the start of the first efflorescence ("d_x") (first ERH: closed circles); and due to the mutual efflorescence of the remnant eutonic compositions (second ERH: open circles) ("d") compared to that of the partially effloresced particles ("d_x").

(A)

(B)
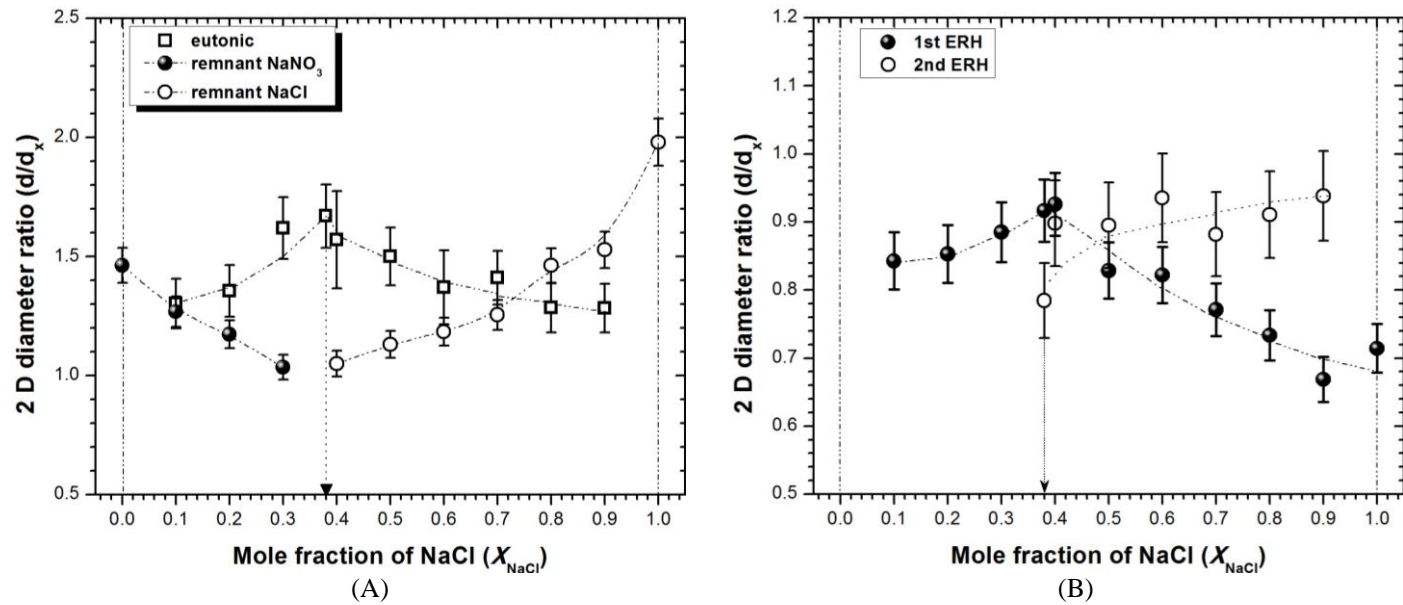
Figure 7. Hygroscopic growth factors in terms of the 2D diameter ratios (d_{95}/d_0, where $d_{95} \equiv$ the diameter at ~ 95%, determined by extrapolation, and $d_0 \equiv$ dry diameter at lowest or ~3% RH) are plotted as a function of the mole fraction of NaCl for the NaCl-NaNO$_3$ mixture particles.